Biochimica et Biophysica Acta 1843 (2014) 2037–2054

Contents lists available at ScienceDirect

Biochimica et Biophysica Acta

journal homepage: www.elsevier.com/locate/bbamcr

Snail1 induced in breast cancer cells in 3D collagen I gel environment suppresses cortactin and impairs effective invadopodia formation

Mi-Sook Lee [a], Sudong Kim [b], Baek Gil Kim [c], Cheolhee Won [d], Seo Hee Nam [e], Suki Kang [c], Hye-Jin Kim [a], Minkyung Kang [f], Jihye Ryu [a], Haeng Eun Song [a], Doohyung Lee [a], Sang-Kyu Ye [d,f], Noo Li Jeon [b], Tai Young Kim [a], Nam Hoon Cho [c], Jung Weon Lee [a,e,*]

[a] Department of Pharmacy, Research Institute of Pharmaceutical Sciences, Tumor Microenvironment Global Core Research Center, Medicinal Bioconvergence Research Center, College of Pharmacy, Seoul National University, Republic of Korea
[b] School of Mechanical and Aerospace Engineering, Seoul National University, Republic of Korea
[c] Department of Pathology, Yonsei University College of Medicine, Seoul 120-752, Republic of Korea
[d] Department of Pharmacology, College of Medicine, Seoul National University, Seoul 151-742, Republic of Korea
[e] Interdisciplinary Program in Genetic Engineering, Seoul National University, Republic of Korea
[f] Department of Biomedical Sciences, College of Medicine, Seoul National University, Seoul 151-742, Republic of Korea

ARTICLE INFO

Article history:
Received 29 November 2013
Received in revised form 14 May 2014
Accepted 16 May 2014
Available online 24 May 2014

Keywords:
3D collagen
JNK
Cortactin
Invasion
Snail1

ABSTRACT

Although an *in vitro* 3D environment cannot completely mimic the *in vivo* tumor site, embedding tumor cells in a 3D extracellular matrix (ECM) allows for the study of cancer cell behaviors and the screening of anti-metastatic reagents with a more *in vivo*-like context. Here we explored the behaviors of MDA-MB-231 breast cancer cells embedded in 3D collagen I. Diverse tumor environmental conditions (including cell density, extracellular acidity, or hypoxia as mimics for a continuous tumor growth) reduced JNKs, enhanced TGFβ1/Smad signaling activity, induced Snail1, and reduced cortactin expression. The reduced JNKs activity blocked efficient formation of invadopodia labeled with actin, cortactin, or MT1-MMP. JNKs inactivation activated Smad2 and Smad4, which were required for Snail1 expression. Snail1 then repressed cortactin expression, causing reduced invadopodia formation and prominent localization of MT1-MMP at perinuclear regions. MDA-MB-231 cells thus exhibited less efficient collagen I degradation and invasion in 3D collagen I upon JNKs inhibition. These observations support a signaling network among JNKs, Smads, Snail1, and cortactin to regulate the invasion of MDA-MB-231 cells embedded in 3D collagen I, which may be targeted during screening of anti-invasion reagents.

1. Introduction

During metastasis, cancer cell migration and invasion are dynamically regulated by coordinated signaling pathways that respond to the extracellular matrix (ECM) or soluble factors of the tumor microenvironment [1]. Invasion involves degradation of the ECM via formation of invasive morphological features including invadopodia, which sense the ECM around the edges of a cell and involve adhesion-dependent signaling activities [2,3]. The formation of invasive features involves dynamic actin remodeling. c-Src-mediated cortactin phosphorylation causes activation of Arp2/3, consequently leading to actin branching and polymerization at lamellipodia and invadopodia [4]. Therefore, cell migration, invasion, and the formation of invasive morphological features could be targets to prevent cancer metastasis. However, investigating the mechanisms behind certain cell behaviors is critical for developing more effective targeted-therapies. While informative, studies investigating the effects of extracellular cues on cell functions in two dimensional (2D) conditions may not relate to the *in vivo* or *in situ* behaviors of cancer cells, because cancer lesions are exposed to a 3D microenvironment [5,6].

Cell behaviors, including migration and invasion, are often investigated in a 2D environment. Although the significance of the tumor microenvironment in promoting tumorigenesis and metastasis has been suggested in many *in vitro* and *in vivo* studies [7], studies evaluating cells in a 2D environment are limited to mimic *in vivo* tumor lesions, whereas embedding cells in a 3D environment allows for the cells to receive and respond to environmental cues like *in vivo* situation. The tumor microenvironment includes ECM proteins, neighboring cells, and soluble factors consisting of growth factors, cytokines, and chemokines, which influence cancer cell function and behavior and have been targeted for clinical treatment [8]. Various environmental stressors including ECM stiffness, extracellular acidity, and intratumoral hypoxia can affect cancer cells and neighboring stromal fibroblasts and inflammatory cells eventually leading to metabolic alterations and the stimulation of mitogenic and survival signaling pathways [9].

* Corresponding author at: Department of Pharmacy, College of Pharmacy, Seoul National University, 1, Gwanak-ro, Gwanak-gu, Seoul 151-742, Republic of Korea. Tel.: +82 2 880 2495; fax: +82 2 872 1795.
E-mail address: jwl@snu.ac.kr (J.W. Lee).

http://dx.doi.org/10.1016/j.bbamcr.2014.05.007
0167-4889/

Studies evaluating cells in a 2D environment are limited in their ability to mimic *in vivo* tumor lesions, whereas embedding cells in a 3D environment allows for the cells to receive and respond to environmental cues like in an *in vivo* situation. Although an *in vitro* 3D environment cannot completely mimic the *in vivo* tumor site, studying the mechanistic behaviors of cancer cells in a 3D environment is beneficial for clinical and pharmaceutical purposes.

c-Jun N-terminal kinases (JNKs) consist of 3 isoforms and are activated by various extracellular cytokines and chemical or radiant stresses [10,11]. JNKs phosphorylate Ser63 of c-Jun leading to its stabilization and transcriptional activation [12,13]. Activated c-Jun can regulate expressions of diverse molecules related to tumor metastasis [14]. Snail1 is a transcriptional repressor to regulate diverse E-box motif-containing molecules for tumor metastasis including E-cadherin [15,16]. Such Snail1- and Snail2/Slug-mediated suppression of E-cadherin is generally accepted as one of the hallmarks of epithelial–mesenchymal transition (EMT), which converts almost static epithelial cells to motile and invasive mesenchymal cells during tumor metastasis [17].

In this study, we evaluated whether and how the invasive behaviors of MDA-MB-231 breast cancer cells embedded in a 3D collagen I gel could be regulated. Exposing the MDA-MB-231 cells to various environmental parameters during culture in the 3D collagen gels decreased JNKs signaling activity (i.e., decreased Ser63 phosphorylation of c-Jun, pS^{63}c-Jun), activated TGFβ1/Smads signaling, enhanced Snail1 expression levels, and reduced cortactin expression levels. Inactivation of the JNKs signaling pathway led to the Smad2/Smad4-activation-mediated expression of Snail1, which in turn suppressed cortactin. As a result, invadopodia formation was less efficient within the 3D collagen I gels, further with cortactin and/or membrane type I matrix metalloproteinase (MT1-MMP) localization at perinuclear regions, leading to less migration and invasion. Therefore, the signaling network consisting of JNKs, Smads, Snail1, and cortactin was revealed to modulate migration and invasion of the MDA-MB-231 cells embedded in 3D collagen I gel.

2. Materials and methods

2.1. Cells, plasmids, and siRNAs

MDA-MB-231, MDA-MB-436, MDA-MB-468, T47D, BT549, Hs578T, and MCF7 breast cancer cells were obtained from the American Type Culture Collection and grown in complete RPMI-1640 (JBI, Daegu, Korea) supplemented with 10% fetal bovine serum (FBS, Life Technologies, Carlsbad, CA) and antibiotics (Life Technologies). DNA plasmids: pcDNA3-DN-JNK1, pcDNA3-Flag-Snail1 WT (a kind gift from Dr. Semi Kim, KRIBB, Korea), pmCherry-MT1-MMP (a kind gift from Dr. Philippe Chavrier, CNRS, France), or pcDNA3.1-GFP-cortactin WT (a kind gift from Dr. Laszlo Buday, Semmel Weis University, Hungary) were transfected into cells 1 day before the cells were embedded in 3D collagen type I gel (PureCol, Advanced BioMatrix, San Diego, CA). Some cells were co-transfected with fluorescein conjugated SignalSilence® control siRNA and SignalSilence® SAPK/JNK siRNA (Cell Signal Technology, Danvers, MA) or On-Target plus Smartpool siRNA duplexes designed to target human Snail1 (NM_005985, Dharmacon, Lafayette, CO). As a negative control, cells were transfected with nonspecific siRNA pool (Dharmacon). All cDNA vectors or siRNA transfections were performed with Lipofectamine™ 2000 (Invitrogen) according to the manufacturer's instructions.

2.2. Polydimethylsiloxane device fabrication

A polydimethylsiloxane prepolymer (PDMS, Sylgard 184, Dow Corning, Midland, MI) was made using a 10:1 (w/w) mixture of PDMS base and curing agent. The PDMS prepolymer was cast against the master and thermally cured to obtain a negative replica-molded piece. After separation from the master, 4- or 8-well chambers were punched out of the molded PDMS with an 8 mm biopsy punch. The PDMS devices and glass coverslips were cleaned with residue-free tape and a N_2 gas air gun, and then treated with oxygen plasma for 45 s to form covalent bonding between them. To restore hydrophobicity to the PDMS after plasma treatment, the devices were kept in a 60°C dry oven for at least 24 h and sterilized by UV irradiation before use.

2.3. Antibodies and reagents

Antibodies and reagents were obtained from the following sources: Sigma-Aldrich, 10× RPMI, anti-α-tubulin, anti-α-SMA, and anti-vimentin; BD Biosciences, anti-cortactin mAb (4F11), anti-human HIF-1α, and BD Matrigel™ Basement Membrane Matrix; Cell Signal Technology, anti-E-cadherin (24E10), anti-Snail1 mAb (L70G2), anti-Smad2/3, anti-phospho-Smad2, anti-phospho-Smad4, anti-pS^{63}c-Jun, anti-c-Jun, and anti-phospho-MAPKAPK-2 (Thr222) antibodies; Millipore, anti-MT1-MMP mAb (MAB3328) and anti-cortactin (p80/85) antibodies (4F11), and Alexa Fluor® 488; Santa Cruz Biotechnology, Inc., anti-JNK rabbit pAb, anti-Arp2 (H-84), and mDia1 (H-58); Invitrogen, diaminophenylindole (DAPI), and rhodamine phalloidin; Jackson ImmunoResearch Laboratories, HRP-conjugated secondary antibodies; LC Labs, SP600125, U0126, and SB203580; Advanced BioMatrix, PureCol type I bovine collagen solution (3.2 mg/ml); PeproTech, TGFβ1; R&D Systems, anti-E-cadherin and anti-TGFβ(1,2,3) antibodies (MAB1835).

2.4. Cell culture in three-dimensional type I collagen gels

3D collagen type I gels were prepared using PureCol type I bovine collagen (Advanced BioMatrix, Poway, CA) in 24-well culture plates. Collagen I mixtures (2.5 mg/ml) were prepared by adding the appropriate volumes of 10× reconstitution buffer (260 mM sodium bicarbonate and 200 mM HEPES) and 10× RPMI (Sigma Aldrich). To adjust the pH of the collagen solution, an ice-cold solution of 2 N NaOH was used for pH 7.2–7.4. The neutralized collagen solution was incubated on ice for 3–5 min to allow the pH to equilibrate, and then the solution was centrifuged for 3 min at 10,000 ×*g* at 4°C to eliminate air bubbles. The bottom layer of 2.5 mg/ml collagen I was made in each well with 30 μl and allowed to gel by incubating for 30 min at 37°C. A top layer was loaded onto the bottom layer using a cell suspension containing 300,000 cells that had been mixed with 150 μl of neutralized collagen mixture and allowed to gel by incubation for 30 min at 37°C. In case of a lower density, 100,000 cells/well were embedded. 3D Matrigel (BD Biosciences, 10 mg/ml) or a mixture of Matrigel and collagen I gel (at a ratio of 5 mg/ml and 1.25 mg/ml, respectively) was also prepared using the same procedure as above. A medium with 10% FBS was then overlaid every day on top of the gel with or without SP600125 (50 μM) for 24–72 h to accelerate the 3D culture-mediated c-Jun inhibition. In cases, a pH-controlled medium (using filtered 1 N HCl) with 10% FBS was replenished every day for 2 days after the embedding, or hypoxic condition at 5% O_2 was applied for 4 h after the embedding, in parallel to the normal condition.

2.5. Immunoblotting

Whole cell lysates from 2D cultures were prepared, as described previously [18]. Cells embedded into 3D collagen I and cultured for 3 days were transferred into ice-cold 1.7 ml tubes and centrifuged at 2500 ×*g* for 1 min to remove residual medium. Cell pellets within collagen I masses were washed with ice-cold PBS and then homogenized using truncated pipette tips (3 times × 20 min on ice) in a modified RIPA buffer (50 mM Tris–HCl, pH 7.4, 150 mM NaCl, 1% NP-40, and 0.25% sodium deoxycholate) with a protease inhibitor cocktail (GenDepot, USA). The extracts were centrifuged for 30 min at 15,000 ×*g* and 4°C. The samples were normalized for equal protein loading in standard immunoblots via α-tubulin levels.

2.6. 3D immunofluorescent analysis

Cells were cultured within polydimethylsiloxane prepolymer (PDMS) glass coverslips and fixed directly with 4% formaldehyde for 30 min at room temperature (RT), and subsequently treated with 100 mM glycine to quench residual aldehyde groups. The cells transfected with GFP or GFP-tagged cortactin for 24 h were embedded into 3D collagen I gels for another 24 h with treatment of either DMSO or SP600125 (50 μM). After PBS washings, cells were permeabilized for 30 min with 0.5% Triton X-100 at RT and blocked for 2 h with PBS in 3% BSA. In cases, cells were stained with either fluorescein-labeled phalloidin (Molecular Probes, 1:250) or Alexa Fluor® 488-labeled anti-cortactin (Millipore, 1: 200) at 4°C overnight. In cases, FITC-collagen I (Sigma, 1 mg/ml) was mixed with collagen I mixtures (2.5 mg/ml) at a 1:8 ratio, prior to embedding cells into the gels consequently for visualization of collagen I fibers. Cells were then washed with washing buffer (130 mM NaCl, 13 mM Na_2HPO_4, 3.5 mM NaH_2PO_4, pH 7.4). Nuclei were counterstained with DAPI. Confocal images were captured at 37°C using a confocal microscope with a Nikon Plan-Apochromat 60×/1.4 N.A. oil objective (Nikon eclipse Ti; Nikon, Japan) and analyzed using the NIS software (Nikon) or IMARIS imaging software (Bitplane AG, Zurich, Swiss). Confocal z-stack images obtained from NIS software were reconstructed into 3D images with the aid of the IMARIS software, Easy 3D modes. The visualization or quantitative colocalization analysis of certain images was performed using the ImarisColoc and surpass module. The graphs were presented as mean ± standard deviation from three independent experiments.

2.7. Time-lapse cell images

Time-lapse cell images of 3D type 1 collagen gels were captured at 37°C with IX81-ZDC (Olympus, Japan) for 24 h, using cells embedded in 3D collagen gels in the absence (control) or presence of 50 μM SP600125 on PDMS glass coverslips. In some cases, cells expressing GFP or mCherry protein were imaged with a confocal Nikon eclipse Ti microscope with a Nikon Plan-Apochromat 60×/1.4 N.A. oil objective. All microscopes were equipped with a Chamlide Incubator system (Live Cell Instrument (LCI), Korea), and an environmental chamber mounted on the microscope was maintained constantly at 37°C, 5% CO_2 and 95% humidity.

2.8. ECM degradation assay using DQ™-collagen I

MDA-MB-231 cells (1.5×10^5 cells/ml per well in the PDMS device) transiently transfected with mCherry-tagged MT1-MMP or mCherry vector for 48 h were embedded into 3D gels consisting of collagen type I (2.5 mg/ml, PureCol) and DQ™-collagen type I (2.5 mg/ml, Life Technologies) at a volume ratio of 10:1. After 30 min incubation at 37°C, each gel in the devices was overlayed with 200 μl RPMI-1640 medium with DMSO (control) or SP600125 (50 μM) treatment. Then 2–4 h later, the z-stack images of up to 3 μm with a 0.7 μm spacing were obtained for 4 h with a 10 min interval, using the Nikon Plan-Apochromat 60×/1.4 N.A. objective of a Nikon eclipse Ti microscope.

2.9. RT-PCR and quantitative real time PCR (qPCR)

Total RNA was extracted from cells in 3D collagen gels using TRIzol (Invitrogen) according to the manufacturer's protocol. One microgram of total RNA was reverse transcribed using amfiRivert Platinum cDNA Synthesis master mix (GenDepot, USA), and qPCR was performed using DreamTaq Green PCR Mater Mix (Thermo Scientific) and the 7900HT Fast real time system (Applied Biosystems). Primers for *Snail1*, *cortactin*, *JNK1*, *Smad2/3*, *Twist*, *Snail2/Slug* and *GAPDH* mRNAs were designed using Primer3 software. Primer sequences were as follows: *CDH1* (*E-cadherin*), forward 5′-TGCCCAGAAAATGAAAAAGG-3′ and reverse 5′-GTGTATGTGGCAATGCGTTC-3′; *CTTN*, forward 5′-CCTGGAAATTCCTCATTGGA-3′ and reverse 5′-CACAAAATCAGGGTCGGTCT-3′; *JNK1*, forward 5′-TTGGAACACCATGTCCTGAA-3′ and reverse 5′-ATGTACGGGTGTTGGAGAGC-3′; *Snail1*, forward 5′-GGTTCTTCTGCGCTACTGCT-3′ and reverse 5′-TAGGGCTGCTGGAAGGTAAA-3′; *Smad2*, forward 5′-CGAAATGCCACGGTAGAAAT-3′ and reverse 5′-CCAGAAGAGCAGCAAATTCC-3′; *Smad4*, forward 5′-CCCCAGAGCAATATTCCAGA-3′ and reverse 5′-GGCTCGCAGTAGGTAACTGG-3′; *Twist*, forward 5′-GGAGTCCGCAGTCTTACGAG-3′ and reverse 5′-TCTGGAGGACCTGGTAGAGG-3′; *slug*, forward 5′-GGGGAGAAGCCTTTTTCTTG-3′ and reverse 5′-TCCTCATGTTTGTGCAGGAG-3; *GAPDH*, forward 5′-GAGTCAACGGATTTGGTCGT-3′ and reverse 5′-GACAAGCTTCCCGTTCTCAG-3′.

2.10. ChIP analysis

The MDA-MB-231 cells were embedded in 3D collagen and cultured in the absence (control) or presence of SP600125 (50 μM) for 3 days. Cell culture medium was removed and the cells in 3D collagen were fixed with 3.7% formaldehyde for 30 min at RT and washed with 100 mM glycine and PBS. The fixed cells were transferred to 1.5 ml centrifuge tubes on ice and washed with ice-cold PBS including protease inhibitor cocktails and centrifuged at 5000 ×*g* for 1 min at 4°C. The supernatants were removed and the cells were lysed with SDS buffer (1% SDS, 10 mM EDTA, 50 mM Tris, pH 8.1 and 1 mg/ml each of aprotinin, leupeptin, and pepstatin A) on ice. Samples were sonicated 6 times on ice (30 s each time at intervals of 1 min) to homogenize cells in the collagen gel, and spun down at 15,000 ×*g* at 4°C for 3 min to remove collagen prior to collection of the supernatants. Aliquoted supernatants (400 μl) were sonicated on ice to fragment DNA to 200–1000 base pair length and centrifuged for 10 min at 15,000 ×*g* and 4°C. The sonicated samples were diluted 10-fold in ChIP buffer (0.01% SDS, 1.1% Triton X-100, 1.2 mM EDTA, 16.7 mM Tris, pH 8.1, 167 mM NaCl, and 1 mg/ml each of aprotinin, leupeptin, and pepstatin A). The diluted chromatin solutions (400 μl) were incubated with 10 μl antibody of anti-pS^{63}c-Jun, anti-Smad2, anti-Smad4, or anti-Snail1 antibody at 4°C with rotation overnight. Before immunoprecipitation, 400 μl of chromatin solution was saved (input chromatin). The immune complexes were collected by adding 50 μl of salmon sperm DNA/protein A and G-beads and rotating for 4 h at 4°C. The beads were recovered by brief centrifugation, washed with low salt complex wash buffer (0.1% SDS, 1% Triton X-100, 2 mM EDTA, 20 mM Tris–HCl, pH 8.1, 150 mM NaCl), high salt complex wash buffer (0.1% SDS, 1% Triton X-100, 2 mM EDTA, 20 mM Tris–HCl, pH 8.1, 500 mM NaCl), LiCl immune complex buffer (0.25% LiCl, 1% NP-40, 1% sodium deoxycholate, 1 mM EDTA, 1 mM EDTA, 10 mM Tris–HCl, pH 8.1), and TE buffer (20 mM Tris, 1 mM EDTA, pH 8.0), with a brief centrifugation between each wash to recover the beads. The immune complexes were eluted from the beads by the addition of 500 μl 1% SDS in 0.1 M $NaHCO_3$ to the bead pellet, vortexing and rotating at 4°C for 10 min. To reverse the cross-linking process, 200 mM NaCl was added to the eluates before incubation at 65°C overnight. Incubation at 55°C for 1 h was performed in 10 mM EDTA, 40 mM Tris–HCl, pH 6.5, and 2 ml of 10 mg/ml proteinase K. DNA was recovered by phenol/chloroform extraction and ethanol precipitation. Promoter sequences were detected in immunoprecipitated and input DNA by PCR using the following primers: *Snail1*, forward primer 1 (*Snail1*-p1) 5′-TCCAAACTCCTACGAGGC-3′ and reverse primer 1 5-′GAAGAAGTGGCAACTGCT-3′, forward primer 2 (*Snail1*-p2) 5′-GGAGACGAGCCTCCGATT-3′ and reverse primer 2 5′-CAGTAGCGCAGAAGAACCACT-3′, and forward primer 3 (*Snail1*-p3) 5′-AGCACACTTCCCTTTGCATT-3′ and reverse primer 3 5′-CACCCGTTCCTTCCCTTATC-3′; primer for negative control regions (*Snail1*-n), forward 5′-CGTAAACACTGGATAAGG-3′ and reverse 5′-GGAAACGCACATCACTGG-3′; primer for the *CTTN*, forward primer (*cortactin*-p) 5′-TCTGCAGACTCGCCACAG-3′ and reverse 5′-CAGGCACCAGGCTCTACTTC-3′; primer for negative control regions (*cortactin*-n), forward 5′-AGTGTTATGATTACAGGC-3′ and reverse 5′-ATAGAGCACAGCGAAGAC-3′.

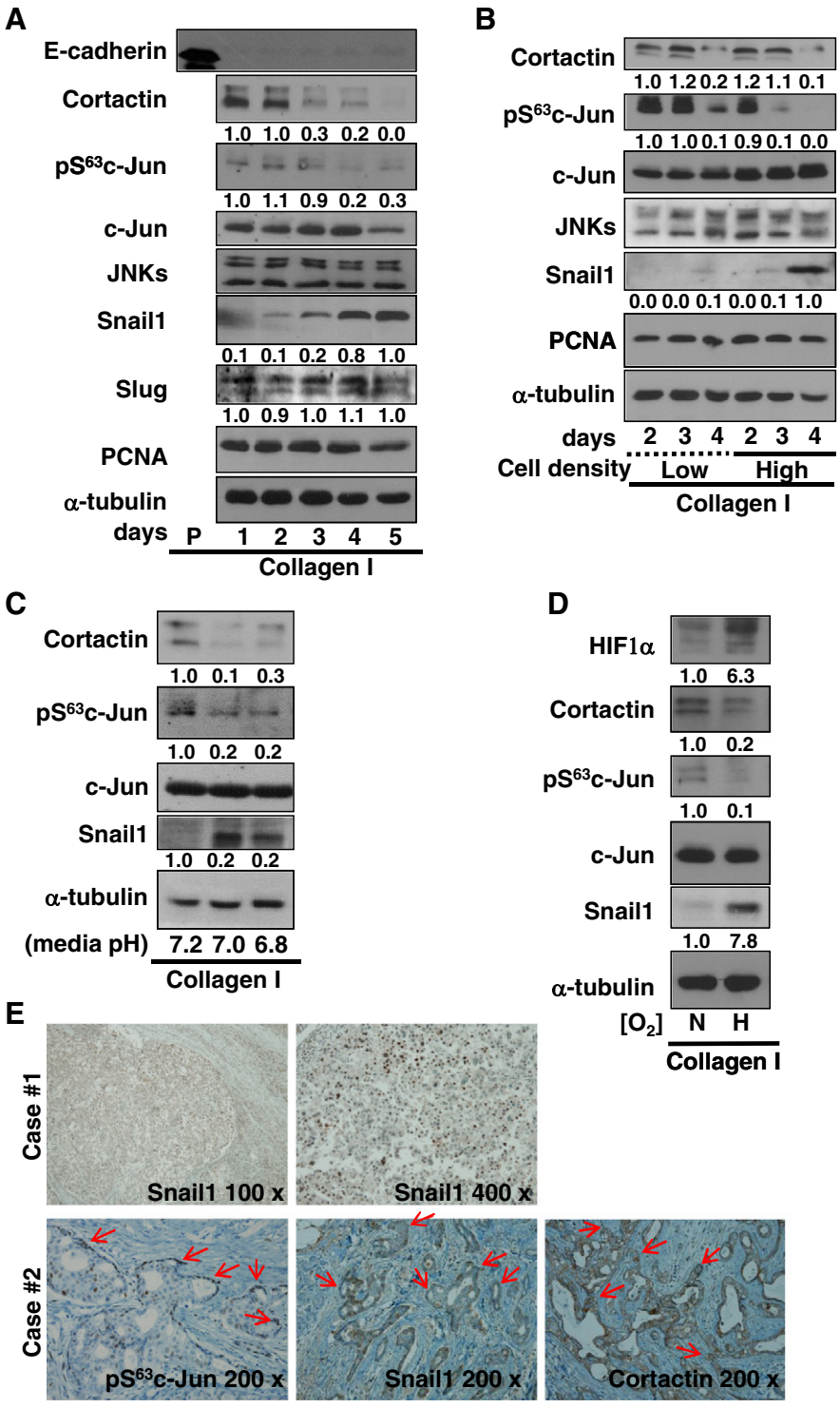

Fig. 1. Diverse tumor microenvironmental factors caused JNK signaling inactivation, Snail1 induction, and cortactin suppression. (A to D) Whole cell lysates were prepared from MDA-MB-231 cells embedded in 3D collagen gels with the normal serum-containing culture medium refreshment every day for up to 5 days (A) and up to 4 days of culture at lower or higher densities (B), in different-pH medium that was replenished every day (C), in hypoxic condition for 4 h (D). N depicts normoxia and H depicts hypoxia. Cell lysates were processed for standard immunoblotting to analyze the indicated molecules. The relative ratio values of band intensities were presented after normalizations to total protein (in case of phospho-protein) or α-tubulin. Data represent three independent experiments. (E) Snail1, pS^{63}c-Jun, and cortactin were immunostained for different regions (e.g., core tumor region or marginal invasive regions) of each patient tissue case (magnifications of 100×, 200×, or 400×). Red arrows indicate invasive margins especially with strong nuclear pS^{63}c-Jun, weak Snail1, and strong cortactin stainings.

2.11. Electrophoretic mobility shift assay (EMSA) and supershift assay

EMSA was performed using nuclear extracts from MDA-MB-231 cells embedded in 3D collagen gels. Cell pellets without cytosolic parts were resuspended in hypertonic buffer C (50 mM HEPES pH 7.9, 50 mM KCl, 300 mM NaCl, 0.1 mM EDTA, 1 mM DTT, 0.1 mM PMSF, and 10% glycerol). The nuclear extracts were then centrifuged for 10 min at 12,000 ×*g*. The oligonucleotide (28-mer, 5′-TAGCGCTTAGCC

AGCTGCGGGCGGACCC-3′) corresponding to the E-box of the human *cortactin* promoter was end-labeled with [γ-^{32}P]ATP using T4 polynucleotide kinase and was purified on a Nick column (Amersham Pharmacia Biotech, Buckinghamshire, UK). The nuclear protein (15 μg) was mixed with 4 μl of concentrated incubation buffer (10 mM Tris–HCl, pH 7.5, 100 mM NaCl, 1 mM DTT, 1 mM EDTA, 4% glycerol, and 0.1 mg/ml sonicated salmon sperm DNA), and the hypertonic buffer was added to make up the final volume to 20 μl. After pre-incubation at room temperature (RT) for 15 min, the labeled probe (400,000 cpm) was added to the nuclear extracts and incubated for an additional 50 min at RT. To ensure the specific binding of the labeled oligonucleotide to nuclear protein, a competition assay was carried out with the 100 nM unlabeled cold oligonucleotide. After the incubation, 0.1% Bromophenol Blue (2 μl) was added, and Snail1–DNA complexes were separated from the unbound free probe by electrophoresis on 6% nondenaturing polyacrylamide gel in 0.5 × TBE (Tris/borate/EDTA) buffer (90 mM Tris base, 90 mM boric acid, and 0.5 mM EDTA, pH 8.0) at 70 V for 2 h. Gels were dried and exposed to X-ray film. For the antibody supershift assay, 1 μl of Snail1 mouse antibody or normal mouse IgG (Cell Signaling Technology, Inc.) was incubated with the nuclear protein extract for 30 min on ice, prior to addition of the reaction mixture containing radiolabeled nucleotides.

2.12. Immunohistochemistry

Normal and tumor breast tissues were obtained from patients in the Yonsei University Hospital (Seoul, Korea) with informed consent. Clinical and biological information was available for the tissue samples. Whole-mount slides of human clinical samples were used for validation of immunoblotting data by immunostaining for Snail1, pS^{63}-c-Jun, and cortactin, as explained previously [19].

2.13. Statistical methods

Band intensities of the Western blots or RT-PCR were measured using Image J to compare each other, which were calculated to give relative ratio values after normalization to total protein (in cases of phospho-proteins), α-tubulin, or *GAPDH* levels. Student's *t*-tests were performed for comparisons of mean values to determine significance. p values <0.05 were considered significant.

2.14. Supplemental information

Supplemental information is found at the Journal website.

3. Results

3.1. Diverse tumor microenvironmental factors revealed a correlation among JNKs inactivation, Snail1 induction, and cortactin suppression

MDA-MB-231 breast cancer cells in 3D collagen gel with 10% serum under different environmental parameters to promote continuous tumor cell growth showed reduced Ser63 phosphorylation levels of c-Jun (i.e., pS^{63}c-Jun), although proliferating cell nuclear antigen (PCNA) was not changed to indicate no significant cytotoxicity during the culture (Fig. 1A). Concomitantly, Snail1 expression increased but cortactin expression decreased, although E-cadherin, Snail2/Slug and c-Jun levels were generally unchanged (Fig. 1A). The increased Snail1 and decreased pS^{63}c-Jun and cortactin levels depended on cell densities, since continuous culture at a high cell density showed more dramatic changes, compared with less cells (Fig. 1B). We then found that extracellular acidity caused the same effect (Fig. 1C). Acute hypoxia with an HIF1α induction showed also the same effect (Fig. 1D). Furthermore, a breast tumor tissue showed Snail1 immunostaining in a random distribution around the distal and proximal edges of a large invasive tumor nest (Fig. 1E, top). Whereas staining of Snail1 was weak (marked with arrows), nuclear pS^{63}c-Jun and cytosolic cortactin stainings were more obvious at the invasive tumor edges of another tumor tissue case (Fig. 1E, bottom). These interestingly suggest an exclusive relationship between Snail1 and cortactin for invasion.

3.2. JNK inhibition caused Snail1 induction and cortactin suppression, leading to reduced migration and invasion in 3D collagen gels

We next examined the morphology and behavior of MDA-MB-231 cells embedded in 3D collagen gels. Pharmacological JNKs inhibition by SP600125 treatment caused an elongation in cellular morphology (Fig. 2A), with a higher length/width ratio (Fig. 2B). However, MDA-MB-231 cells embedded in 3D Matrigel or a mixture of Matrigel and collagen (at a 4:1 w/w ratio) did not show the elongation (Fig. S1A), indicating an ECM-specific morphological effect. RT-PCR and immunoblotting after JNK inhibition showed that *Snail1* and *Twist* mRNA expression increased, but *cortactin* mRNA decreased, although *Snail2*/*Slug* mRNA level was not changed (Fig. 2C). More importantly, the *Snail1* mRNA levels were not correlated with *E-cadherin* (*CDH1*) mRNA or E-cadherin protein levels, indicating that the Snail1 might not be linked to E-cadherin suppression (Fig. 2C). These gene expression changes occurred in the cells embedded only in collagen gel but not Matrigel or the mixture of Matrigel and collagen I (Fig. S1B). Phosphorylated-ERKs and -p38 were not involved in the effects on alterations in gene expression, because there were no similar changes upon JNK inhibition (Figs. 2D, S1C and D). SP600125 treatment did not alter actin nucleator Arp2 and mDia expression levels (Fig. S1D). Thus, the morphological elongation by JNK inhibition might be correlated with the alterations in expression levels of Snail1 and cortactin. We next checked the relationship between the cortactin level and the cellular length by examining whether exogenous cortactin (over)expression abolished the SP600125 treatment-mediated elongation. Whereas cells transfected with GFP alone were elongated by the SP600125 treatment, cells transfected with GFP-cortactin did not show the SP600125 treatment-mediated effects (Fig. 2E).

Live cell imaging was used to monitor morphological changes and/or motility upon treatment with or without SP600125. SP600125-treated cells exhibited relatively-steady locations and morphological protrusions during time-lapse imaging, whereas control cells showed dynamic growth of invasive protrusions and locomotion (Fig. 2F and Supplementary Movies 1 and 2) leading to more consistent migration in 3D collagen gels (Fig. 2G). Therefore, it is possible that JNK inhibition-mediated effects may control migratory and invasive properties of MDA-MB-231 cells in 3D collagen gel.

3.3. JNK inhibition caused less efficient formation of actin and cortactin-enriched invadopodia

When we costained cells with cortactin and F-actin, which are known to localize at the invadopodia [20], images to stain Alexa 488®-tagged anti-cortactin (green) and phalloidin (red) clearly showed more yellowish-overlapped spots (i.e., invadopodia) in control vehicle-treated cells (Fig. 3A) than in SP600125-treated cells (Fig. 3B). The less overlapped spots in SP600125-treated cells than in control cells was demonstrated by quantification of merged yellowish spots in slice images (Fig. 3C). We also observed dynamic turnover in GFP-cortactin localization along the frequently-altered boundaries of control cells, whereas its localization in SP600125-treated cells was steady and not at the cellular boundary (Fig. S2, Supplementary Movies 3 and 4). Further, collagen I degradation by the cells was monitored using DQ ™-collagen I that was mixed into the 3D collagen I gels. Whereas MDA-MB-231 cells treated with DMSO showed more green fluorescent spots for the collagenase activity around leading and base/cell body area, the SP600125-treated cells showed much less (Fig. 3D, Supplementary Movies 5 and 6).

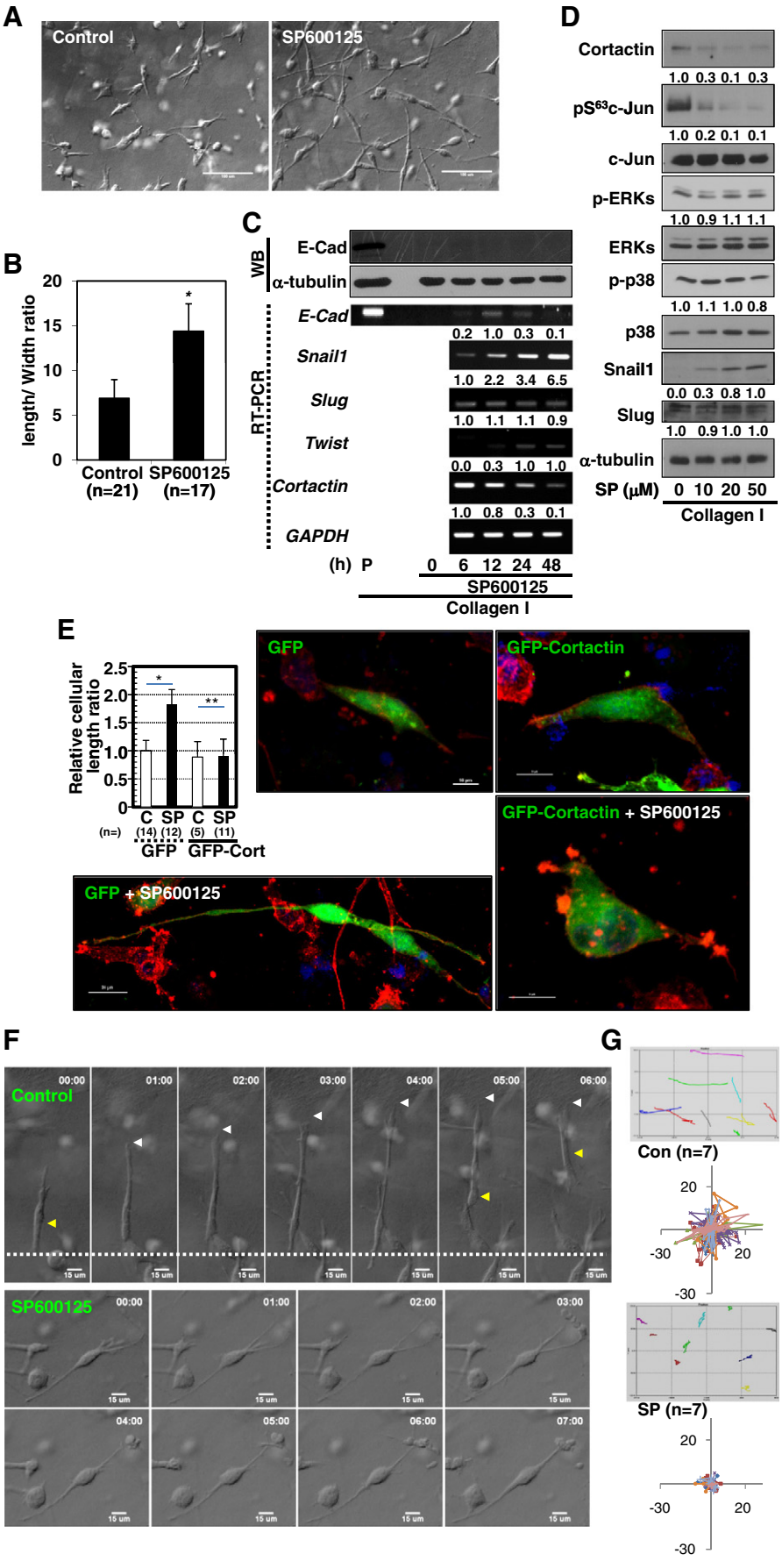
A
Control
SP600125
B
length/ Width ratio
Control (n=21)
SP600125 (n=17)
C
WB
E-Cad
α-tubulin
RT-PCR
E-Cad
Snail1
Slug
Twist
Cortactin
GAPDH
(h) P 0 6 12 24 48
SP600125
Collagen I
D
Cortactin
pS63c-Jun
c-Jun
p-ERKs
ERKs
p-p38
p38
Snail1
Slug
α-tubulin
SP (μM) 0 10 20 50
Collagen I
E
Relative cellular length ratio
C SP C SP
(n=) (14) (12) (5) (11)
GFP GFP-Cort
GFP
GFP-Cortactin
GFP-Cortactin + SP600125
GFP + SP600125
F
Control
SP600125
G
Con (n=7)
SP (n=7)

Human breast cancer cell lines cultured on 3D-laminin-rich ECM gels are grouped into four different morphological classifications: round, mass, grape-like, and stellate [21]. When diverse breast cancer cell lines were tested for the JNK inhibition-mediated effects in the 3D collagen I environment, mass (T-47D and MCF-7) or grape-like (MDA-MB-468) cells did not show morphological elongation, whereas stellate cells (MDA-MB-436 and MBA-MB-231 cells) showed morphological elongation with a loss of cortactin- and actin-colocalized spots (yellow spots) upon JNK inhibition (Fig. 3E). The colocalization of F-actin and cortactin in MDA-MB-436 cells was decreased by SP600125 treatment (Fig. 3F). Further, like MDA-MB-231 cells, MDA-MB-436 cells decreased pS^{63}c-Jun, increased Snail1 expression, and decreased cortactin expression upon JNK inhibition (Fig. 3G). Other basal tumor type cells like BT-549 and Hs578T also showed such morphological elongations and a signaling axis of c-Jun/Snail1/cortactin upon JNK inhibition (Fig. S3). However, MDA-MB-231 and MBA-MB-436 cells did not show altered expressions of EMT markers, including E-cadherin, α-smooth muscle actin (α-SMA), or vimentin (Fig. 3H), although the JNK inhibition caused Snail induction (Fig. 3G). These observations support that certain breast cancer cells (i.e., stellate-grouped cells) could become less invasive by the signaling link between pS^{63}c-Jun, Snail1, and cortactin, irrelevantly to the EMT process.

When Snail1 was overexpressed, cortactin was reduced but pS^{63}c-Jun was not changed (Fig. 4A), suggesting c-Jun upstream of Snail1. Overexpression of Snail1 (marked by cotransfected mCherry plasmid) decreased endogenous cortactin-enriched spots, compared with mCherry alone-transfected control or Snail1-untransfected (i.e., only greenish) cells showing more frequent cortactin-positive spots at the tips and base/cell body area (Fig. 4B, C). Following transfection with siSnail1, *cortactin* (*CTTN*) mRNA increased and *JNK1* mRNA was not changed (Fig. 4D). The JNK inhibition-mediated decrease in cortactin expression was abolished by knockdown of Snail1 (Fig. 4E).

3.4. The relationship among pS^{63}c-Jun, Snail1, and cortactin occurred at the transcriptional level

We next tested whether these molecular changes occurred at the transcriptional level by chromatin immunoprecipitation (ChIP) assay. There found AP1 binding sites in the human *Snail1* gene promoter region and E-box binding sites in the human *cortactin* (*CTTN*) gene promoter region (Fig. 5A). Chromatin extracts, prepared cells in 3D collagen gel in the presence of SP600125 treatment with enhanced Snail1 and reduced pS^{63}c-Jun and cortactin levels (Fig. 5B), were immunoprecipitated with either anti-pS^{63}c-Jun or anti-Snail1 antibody (Fig. 5C, D). PCR product representing region p1 of the *Snail1* promoter (*Snail1*-p1), but not a control region (i.e., a non-AP1-binding site, *Snail1*-n), was only detected from pS^{63}c-Jun-immunoprecipitated chromatin (Fig. 5C), indicating a binding of pS^{63}c-Jun to the *Snail1* promoter region. However, there may be other factors involved in *Snail1* transcription because reduced pS^{63}c-Jun correlated with enhanced *Snail1* mRNA levels (see below). Meanwhile, chromatin precipitated with anti-Snail1 antibody showed more PCR product representing region p of the *CTTN* promoter (*cortactin*-p), but not from a control region in the promoter (*cortactin*-n), in SP600125-treated cells (Fig. 5D). Snail1, a transcriptional suppressor [22], could thus bind a promoter region of the *CTTN* gene and suppress cortactin expression.

RT-PCR revealed that *Snail1* mRNAs were more stable in control cells (treated with actinomycin D alone) than cells treated with actinomycin D and SP600125 together (Fig. 5E). Quantitative real time PCR (qPCR) analysis showed that *CTTN* mRNA had a half-life longer than 48 h in control cells, but a half-life of approximately 24 h in cells treated with both actinomycin D and SP600125 (Fig. 5F). The half-lives of Snail1 and cortactin proteins were <6 h for Snail1 and ≅12 h for cortactin, being independent of SP600125 treatment (Fig. 5G). *In vitro* binding of Snail1 protein from the nuclear extracts of MDA-MB-231 cells in 3D collagen gels to the 5′ promoter of cortactin was analyzed by EMSA using the region covering the E-box sequence as the probe. The probe binding increased as more nuclear extracts were mixed (Fig. 5H, left panel). The binding was abolished by cold probe incubation, and the complex between the probe and Snail1 was confirmed by a supershift when anti-Snail1, but not normal IgG, was added (Fig. 5H, right panels).

pS^{63}c-Jun binding to a *Snail1* gene promoter region occurred without SP600125 treatment. Thus, increased Snail1 transcript upon JNK inhibition indicated that another factor(s) could be involved in *Snail1* transcription. *Snail1* mRNA increased but *CTTN* mRNA decreased in cells cultured in 3D collagen gel, whereas *Smad2* and *Smad4* mRNAs were not altered (Fig. 6A), indicating that cells embedded in 3D collagen gel may secrete TGFβ1 leading to autocrine effects. However, immunoblottings showed increased TGFβ1, Smad2, and Smad3 protein levels and Smad2 phosphorylation (Fig. 6B). JNK inhibition or extracellular acidity also enhanced TGFβ1 and Smad2 expression (Fig. 6C, D). Cells were then analyzed for Snail1 and cortactin expression after transfection with shRNA against GFP or each Smad. The JNK inhibition-mediated changes in Snail1 and cortactin expression were blocked by Smad2 or Smad4 knockdown, whereas Smad3 knockdown did not block the changes (Fig. 6E). SP600125-treated cells showed Smad-binding element in the *Snail1* gene promoter region (*Snail1*-p3), as demonstrated by RT-PCR amplification of chromatin precipitated using anti-Smad2 or -Smad4 (but not -Smad3) antibodies (Fig. 6F), suggesting that TGFβ1/Smad activity in MDA-MB-231 cells embedded into 3D collagen gel might induce *Snail1* transcription, following JNK inhibition.

3.5. JNK1 suppression or Snail1 expression caused the inverse relationship between Snail1 and cortactin expression, and decreased invadopodia formations

To avoid nonspecific effects by SP600125, cells were transfected with GFP plasmids (to mark transfectants during imaging) together with or without dominant-negative (DN) JNK1. DN-JNK1 expression reduced pS^{63}c-Jun, enhanced Snail1, decreased cortactin expression (Fig. 7A), and less actin-enriched spots (shown as peaks in the histogram, Fig. 7B). When JNK1 was suppressed by siRNA introduction, the relationship among JNK1, Snail1, and cortactin levels was similar to that found in MDA-MB-231 cells continuously cultured in 3D collagen gels with SP600125 treatment (Fig. 7C, D). Further, siJNK1-transfected cells (marked with cotransfected GFP-tagged control siRNA as a green spot marked with a white arrow [23]) showed reduced actin-enriched spots, compared with untransfected neighboring cells (i.e., siJNK1-negative cell without green spots, Fig. 7E).

Fig. 2. Inhibition of JNK signaling caused Snail1 induction and cortactin suppression, leading to less dynamic MDA-MB-231 cell migration and invasion within 3D collagen gels. (A and B) Images of elongated morphology of MDA-MB-231 cells in 3D collagen gels after pharmacological inhibition of JNK signaling for 3 days were saved (A) and quantified to get length/width ratio using imaging software. * depicts a statistical significance at $p = 1.65 \times 10^{-6}$ (B). (C) Western blot or RT-PCR analysis from the cells embedded in 3D collagen gels and treated with 50 μM SP600125 for different times. P depicts a positive control of HCT116 colon cancer cell extracts. The relative ratio values of band intensities were presented after normalizations to total protein (in case of phospho-protein), α-tubulin, or *GAPDH*. (D) Immunoblots were performed using whole lysates of cells embedded in 3D collagen gels and treated with SP600125 (SP) at different concentrations for 24 h. (E) Cells were transiently transfected with GFP or GFP-tagged cortactin (GFP-Cort) for 2 days and the cells were then embedded into 3D collagen I gels in the absence (Control, C) or presence of SP600125 (SP), before imaging for rhodamine phalloidin for F-actin (red) and GFP fluorescence. The cellular length in the multiple representative images was measured using IMARIS software. * and ** depict statistical significant and insignificant difference, respectively. (F and G) Time-lapse microscopic images of the cells embedded in 3D collagen gels and treated with vehicle (DMSO, Control) or 50 μM SP600125. Arrowheads in the control condition indicate dynamically and invasively growing tips (F). Tracking analysis of each control cell showed dynamic migration for longer distances (Con, n = 7), but SP600125-treated cells exhibited decreased motilities (SP, n = 7). These snap images were from Supplementary Movies 1 (Control) and 2 (SP600125-treated). The data represent three independent experiments.

3.6. JNK1 inactivation caused localization of MT1-MMP at perinuclear regions but not membrane boundaries

When actin and collagen fibers were stained or visualized, control cells showed clear ECM-degraded areas (yellow arrowheads), whereas SP600125-treated cells showed no clear ECM-degraded areas, as shown as yellow arrowheads especially in the *xz* plane (Fig. 8A). We then imaged the invadopodia using a different marker, matrix metalloproteinase MT1-MMP [20]. When cells transfected with mCherry-tagged MT1-MMP were embedded into 3D collagen gel before double-staining for MT1-MMP (red) and actin (green), MT1-MMP was overlapped with actin-enriched spots, as demonstrated by frequent overlapping throughout the *xz* or *yz* cut-stacks (Fig. 8B). MDA-MB-231 cells embedded in 3D collagen gels did not exhibit changes in MT1-MMP expression, unlike cortactin (Fig. 6C and D). When mCherry-tagged MT1-MMP was transfected into cells, the vehicle-treated control cells showed dynamic turnover of MT1-MMP-positive spots along peripheral and/or central regions of the cells and frequent alterations in morphological boundaries, and led to enhanced cellular locomotion (Fig. 8C, Supplementary Movie 7). However, SP600125-treated cells showed a steady morphology and more MT1-MMP around perinuclear regions than along cellular boundaries (Fig. 8D, Supplementary Movie 8). Cells cotransfected with mCherry-MT1-MMP and GFP-cortactin showed dynamic translocation of spots doubly-positive for cortactin and MT1-MMP (i.e., yellowish spots) along the cellular boundaries (arrowheads, Fig. 8E, Supplementary Movie 9), whereas the cortactin and MT1-MMP double-positive

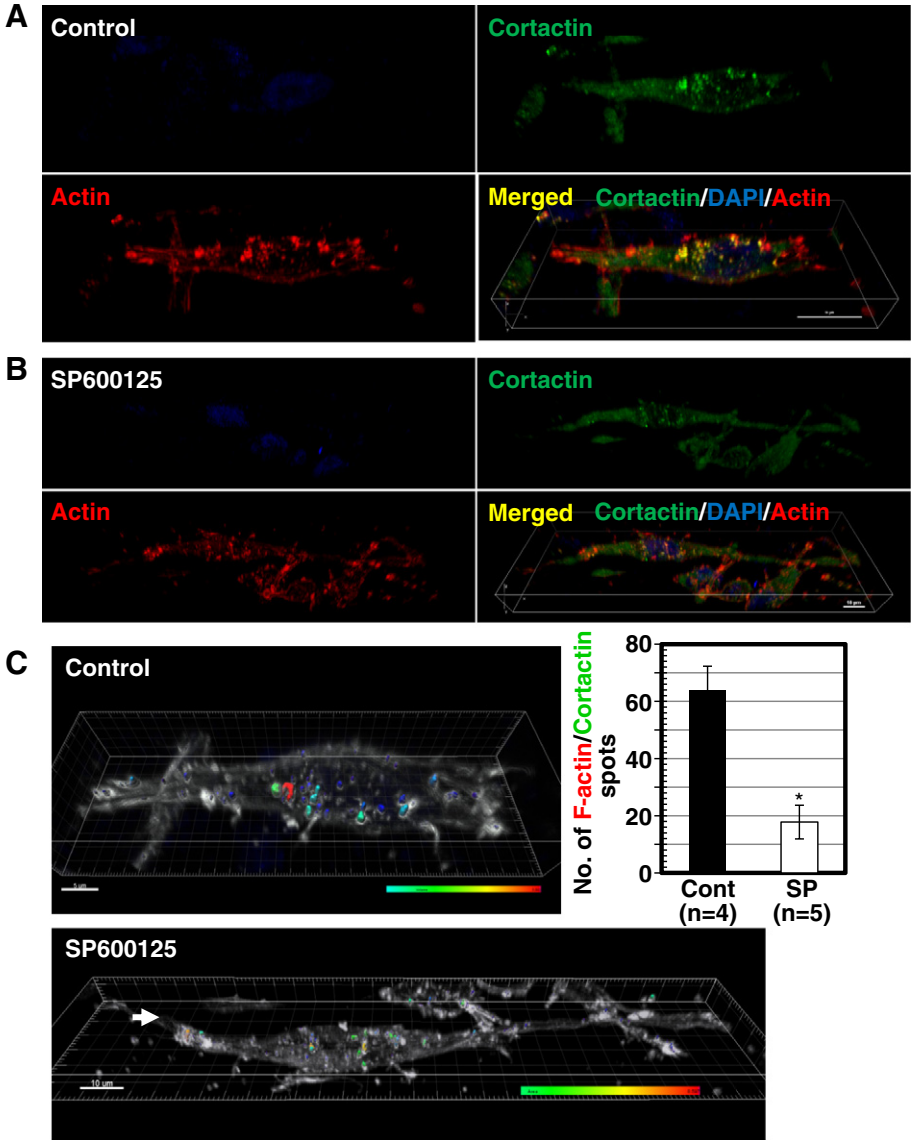

Fig. 3. JNK inhibition-mediated effects among different breast cancer cell lines. (A–C) Confocal fluorescent snap images are shown for MBA-MB-231 cells treated with DMSO (vehicle, Control, A) or SP600125 (B). Confocal images in each channel (green for cortactin and red for F-actin) are shown separately and merged. Fluorescent intensities and superimposition (i.e., colocalization) throughout each plane at the same depth from the ventral boundary were analyzed by IMARIS software. (C) Pseudocolor to show the colocalization ranges from red (highest signal intensity) to dark blue (lowest signal intensity) over the cells in gray. The numbers of spots with colocalized F-actin and cortactin were counted for control ($n = 4$) and SP600125-treated (SP, $n = 5$) cells to present as a quantitative graph at mean ± standard deviation. * depicts a statistical significance of $p < 0.05$. (D) Cells were transiently transfected with mCherry vector alone for 48 h and then embedded into 3D collagen I gels mixed with DQ-collagen I (at a ratio of 10:1) for live collagen degradation analysis in the presence of DMSO (control) or SP600125 treatment. Arrowheads at each color for a separate cell show green fluorescence as the ECM degradation spots. Live images (Supplementary Movies 5 and 6) were collected at a 10 min interval, but snap images at irregular intervals were selectively shown for a clear difference in green spot numbers between the experimental conditions. Images with cells embedded in 3D collagen I gels with vehicle (Cont, $n = 11$) or SP600125 (SP, $n = 8$) treatment were saved to count numbers of collagen degradation spots per cell. The green spots for DQ-collagen I degradations were visually counted and represented as mean ± standard deviation values (graph). * depicts $p < 0.05$ for a statistical significance. (E–H) Different breast cancer cells embedded in 3D collagen were analyzed for F-actin (red), cortactin (green), and nucleus (DAPI) using confocal microscopy at confocal slices (E) for quantifications of MDA-MB-436 cells (F) as shown in Fig. 3C, or immunoblotting for the indicated molecules (G and H). The data represent three different experiments.

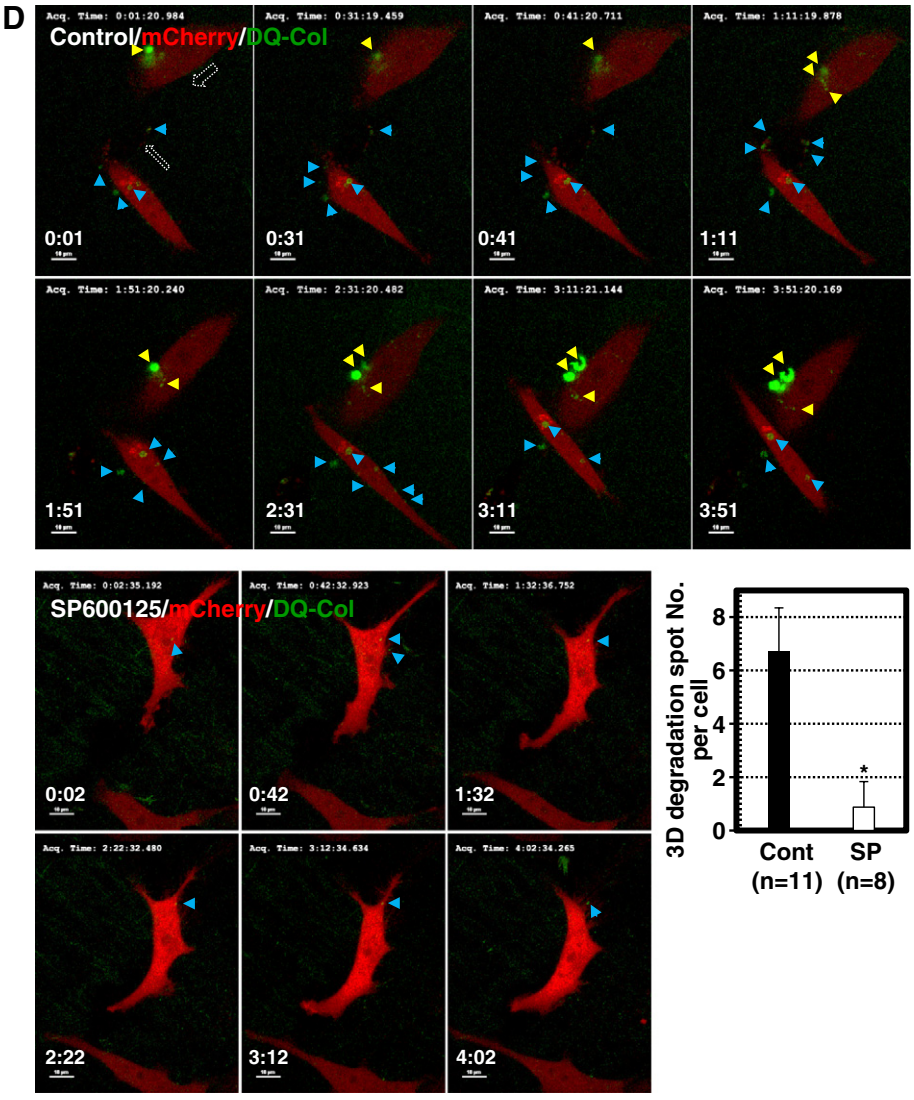

Fig. 3 (*continued*).

spots in SP600125-treated cells were more localized around the nucleus than cell boundaries (Fig. 8F, Supplementary Movie 10). The collagen I degradation of cells transfected with mCherry-tagged MT1-MMP was then examined using DQ™-collagen I. Although the control cells without SP600125 treatment showed dynamic ECM degradation spots costained with MT1-MMP along base/cell body area (blue marked, Supplementary Movie 11), SP600125-treatment reduced the degradation (Fig. 8G and H, Supplementary Movie 12).

4. Discussion

This study revealed that the environmental parameters around tumor cells including cell density, extracellular acidity, and hypoxia could cause JNK signaling inactivation (i.e., decreased c-Jun phosphorylation), TGFβ1/Smad signaling activation, Snail1 induction, and cortactin suppression. This signaling network led to stabilized localization of cortactin and MT1-MMP (both proteins are invadopodia markers) at perinuclear regions rather than at cell membrane boundaries, resulting in the reduced formation of actin and cortactin-enriched invadopodia along the edges of cells embedded in 3D collagen gels. Furthermore, more frequent morphological change and displacement of MDA-MB-231 cells in 3D collagen I gels, compared with SP600125-treated and thereby Snail1-induced MDA-MB-231 cells (Figs. 2 and 8), indicate that the cellular migration and invasion through 3D ECM environment were attenuated by the JNK inhibition-mediated effects. In this study, the use of MDA-MB-231 cells in 3D collagen I more accurately can reflect growth of a tumor in vivo, only in the context of comparing to growth of cells on monolayer 2D culture. Although the tumor microenvironment, including other cells, was not completely available in this experimental assay setup, it might certainly suggest an aspect of tumor cells with autocrine behaviors in 3D, compared with 2D environment.

We have compared the invasive features of MDA-MB-231 breast cancer cells embedded in 3D collagen gels, 3D Matrigel, or a mixture of Matrigel and collagen I (at a 4:1 w/w ratio). Cells embedded in 3D Matrigel or the mixture of Matrigel and collagen I did not exhibit the JNK, Snail1, and cortactin linkage demonstrated in cells embedded in 3D collagen gels. A specific communication between MDA-MB-231 cells and surrounding ECM types appeared to regulate invasive behaviors. Among the diverse morphologically-different breast cancer cells [21], only stellate cells (MDA-MB-231 and MDA-MB-436 with basal B tumor classification) showed JNK activity-dependent morphological elongation and signaling network change, leading to a decreased invadopodia formation, indicating that invasiveness in a certain type

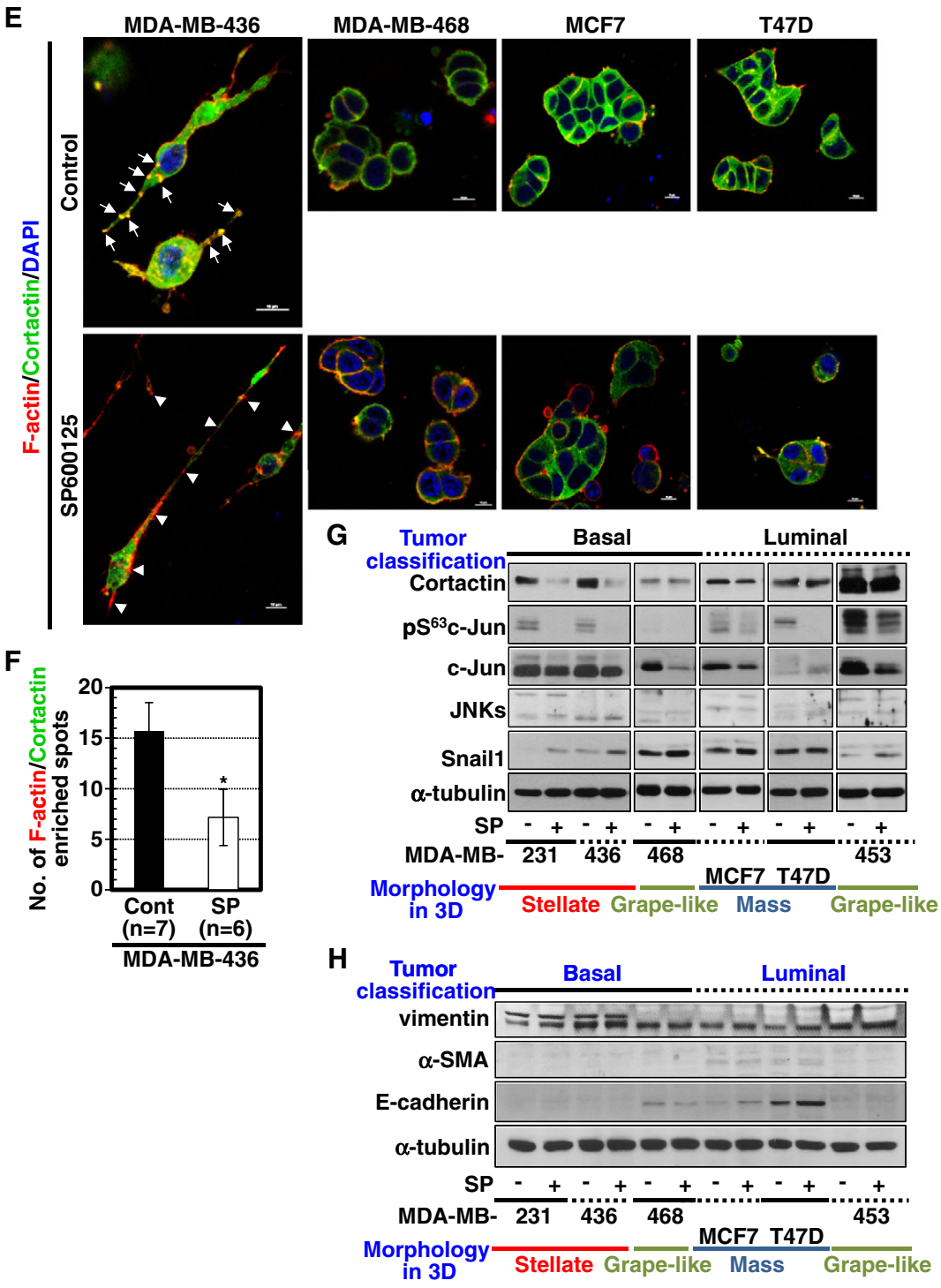

Fig. 3 (*continued*).

of breast cancer cells may be regulated by the JNK, Smads, Snail1, and cortactin network. Meanwhile, mass-grouped cells (T-47D and MCF-7 with luminal tumor classification) that have been established from IDC tumors [21] did not show the JNK-dependent effects on Snail1 induction and cortactin suppression. Grape-like-group cells (MDA-MB-468 with basal A tumor classification and MDA-MB-453 with luminal tumor classification) did not show the JNK-dependent effects. Therefore, it may be likely that a breast cancer cell type with basal B tumor classification and stellate morphology in 3D could be influenced by JNK activity for Snail1 induction and cortactin suppression. Consistent with increased Snail1 stains approaching the central necrotic area of ductal carcinoma *in situ* (DCIS) [24], we here observed cases showing that Snail1 was randomly expressed in clinical breast tumor tissues rather than being localized around the invasive edges, although the cases were rare at approximately 10% rate. The JNK, Smads, Snail1, and cortactin signaling network may be related to a specific breast tumor population. MDA-MB-231 and MDA-MB-436 cells are triple-negative breast cancer cells [negative for estrogen receptor (ER), progesterone receptor (PgR), and HER2 amplification [21]] and further negative for E-cadherin (Fig. 3H). Thus it may be likely that the JNK activity-

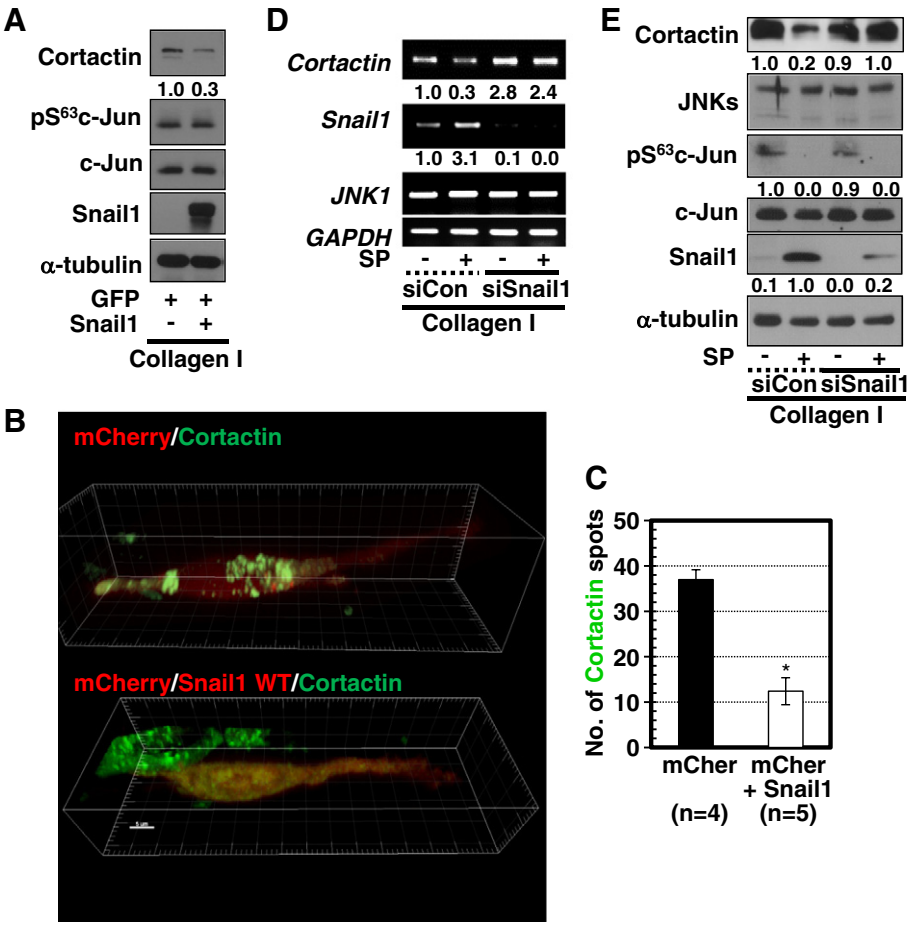

Fig. 4. JNK inhibition-mediated Snail1 expression caused also an inverse relationship between Snail1 and cortactin and decreased actin and cortactin-enriched invadopodia formation. (A–C) Immunoblots (A) or confocal images (B) were collected from MDA-MB-231 cells in 3D collagen I gels transiently transfected with mCherry empty plasmid (mCher) or mCherry plasmid together with Snail1 WT plasmid (red, B). Note that mCherry/Snail1 WT-cotransfected cells (bottom in B) showed less cortactin-enriched spots, compared with cells untransfected with any plasmid (only green, bottom in B) or transfected with mCherry plasmid alone (top in B). The number of endogenous cortactin-enriched spots (visualized by immunostaining with Alexa 488®-tagged anti-cortactin, green) in mCherry-transfected cells was quantified using IMARIS software for a graphic presentation at mean ± standard deviation. * depicts a statistical significance at $p < 0.05$ (C). (D and E) RT-PCR (D) and immunoblots (E) of cells embedded in 3D collagen gels treated with vehicle (−) or SP600125 (SP) after transient transfection with siRNAs against control sequence (siCon) or Snail1 (siSnail1). The relative ratio values of band intensities were presented after normalizations to total protein (in case of phospho-protein), α-tubulin, or *GAPDH*. The data represent three different experiments.

dependent Snail1 induction and cortactin suppression may be limited to a breast cancer cell population without ER, PgR, HER2, and E-cadherin expression.

Snail1 induces also EMT by suppressing E-cadherin [15,25], being associated with the metastatic potential of infiltrating ductal carcinoma (IDC) [26,27]. However, in DCIS, Snail1 is also localized in the nucleus, being correlated with higher tumor grade and proliferation rather than with migration [24], and expressed at similar levels in both the tumor and the normal zone of DCIS tissues [19]. Therefore, Snail1 expression may have differential effects on metastasis depending on the local invasiveness. It is well-known that a small population of breast tumor cells is motile even around the margins of metastatic breast cancer models [28,29]. In this study, Snail1 induced by JNKs inhibition was not correlated with *E-cadherin* (*CDH1*) mRNA suppression, and MDA-MB-231 and MDA-MB-436 cells did not show basal E-cadherin expression. Instead, Snail1 bound the promoter of *cortactin* (*CTTN*) and negatively regulated its expression. Snail1 may thus have different downstream targets leading to less metastatic potential in a specific breast cancer cell population, like DCIS (an early noninvasive breast cancer), rather than leading to E-cadherin suppression and enhanced migration and invasion. Indeed, hypoxia-mediated Snail1 expression in breast cancer cells slightly decreases migration of MDA-MB-231 cells but increases migration of MDA-MB-468 cells, following a partial hypoxia-induced EMT phenotype [24], being consistent with the observations in this study; the phospho-c-Jun/Snail1/cortactin linkage in MDA-MB-231 cells was correlated with JNK-inhibition-mediated less formation of invadopodia in 3D condition, but the linkage was absent in MDA-MB-468 cells due to no basal c-Jun phosphorylation and no change in cortactin level (Fig. 3G). Therefore, it might be likely that Snail1 expression might not be always leading to enhanced migration if the EMT phenotype to suppress E-cadherin is not completely accompanied, as shown in this study that the expression pattern of E-cadherin was irrelevant to that of Snail1 (Figs. 2C, 3G and H).

In control MDA-MB-231 cells in 3D collagen gels, pS^{63}c-Jun bound to the promoter of the *Snail1* gene, indicating that active c-Jun may regulate basal *Snail1* transcription. However, in the conditions where pS^{63}c-Jun decreased via the influence of extracellular environments, Snail1 mRNA and protein levels increased, indicating that proteins others than c-Jun could be involved in *Snail1* transcription. Inhibiting JNK activity in E12.5 lung explants causes TGFβ1-activated Smad2 phosphorylation and gene expression changes for branching morphogenesis [30]. c-Jun associates with the oncoprotein, Ski, to suppress Smad2 transcriptional activity [31]. It may thus be likely that JNK inhibition is coordinated with TGFβ1-activated Smad2/4 binding to the *Snail1* gene promoter region. Although it is reported that TGFβ1 regulates cross-talk between Smad signaling and JNK signaling during EMT of rat peritoneal mesothelial cells [32], there are other reports that c-Jun activity is inversely correlated with TGFβ1 and Smad signaling activity [33,34],

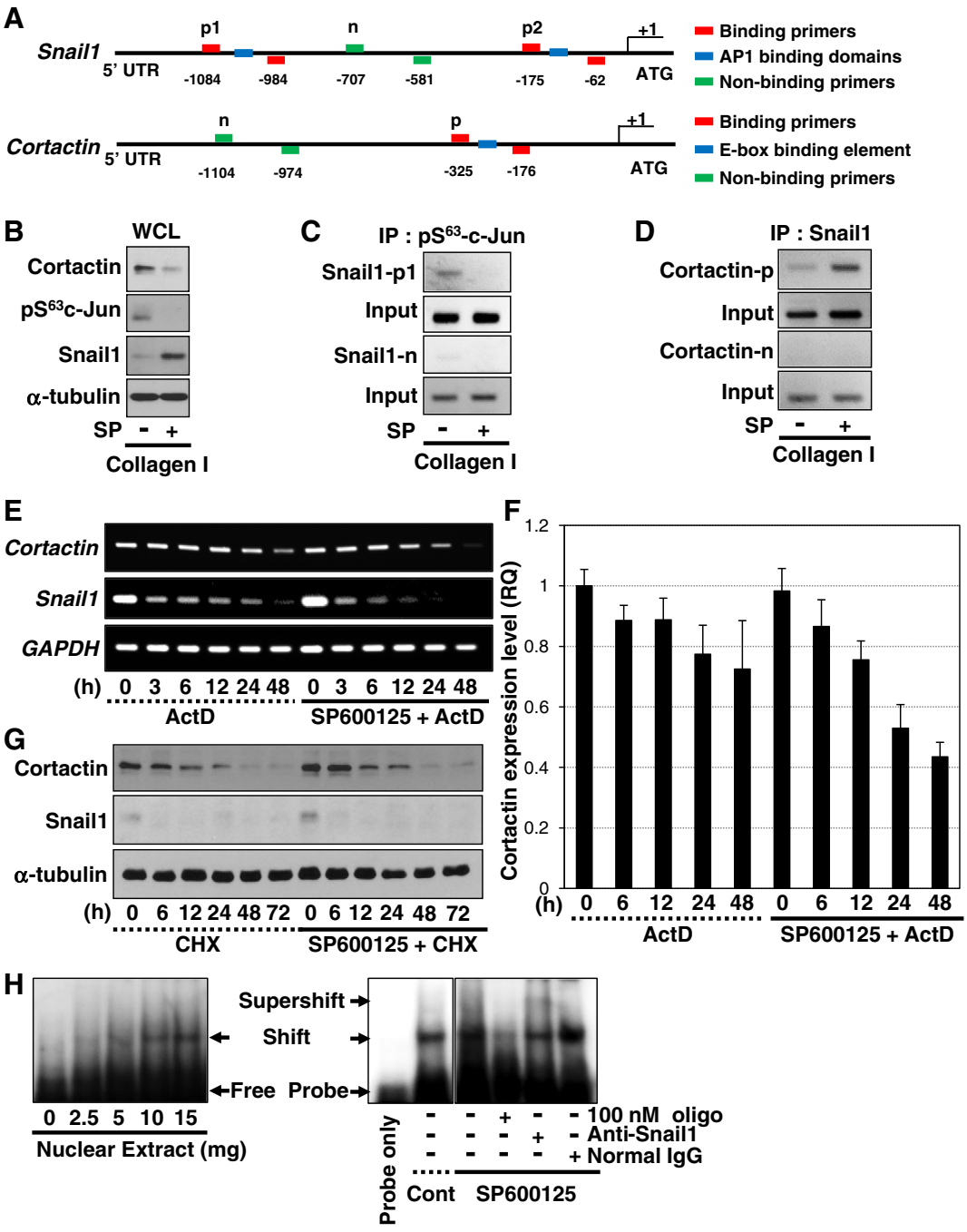

Fig. 5. The relationship between pS^{63}c-Jun, Snail1, and cortactin occurred at the transcriptional level. (A) Schematic presentations of AP1-binding domains in the promoter region of the *Snail1* gene (top) or E-box binding element in the promoter regions of the *CTTN* gene (bottom). (B–D) ChIP assay using chromatin immunoprecipitates using anti-pS^{63}c-Jun antibody (C) or anti-Snail1 antibody (D) prepared from whole cell lysates (WCL, B) of cells treated with vehicle (−) or SP600125 (SP, +) in 3D collagen gels. (E and F) RT-PCR analysis for *Snail1* or *cortactin* (E) or quantitative RT-PCR for *cortactin* (F) from the cells treated with DMSO or SP600125 with or without actinomycin D (ActD). (G) Immunoblotting for Snail1 or cortactin from the cells treated with DMSO or SP600125 with or without cycloheximide (CHX). (H) Nuclear extracts with different protein amounts from cells in 3D collagen I were mixed to [γ-^{32}P]ATP-labeled probe to cover the E-box sequence in the human *cortactin* promoter region during EMSA assay, as explained in Materials and Methods. Alternatively, the nuclear extracts were premixed with cold oligonucleotide probe, anti-Snail1 mAb, or normal mouse IgG, before EMSA assay. The data represent three independent experiments.

in agreement with this study. In 2D condition, Snail1-mediated EMT results in enhanced invasion [35]. The collagen receptor discoidin domain receptor 2 (DDR2) post-transcriptionally stabilizes Snail1 via c-Src and ERKs activations, and facilitates metastasis of breast cancer cells [36]. In the current study, however, enhanced *Snail1* transcription did not involve ERK activity or E-cadherin suppression, but rather led to cortactin suppression and less migration potential. TGFβ1/Smad3-mediated Snail1 induction in pancreatic cancer cells promotes invasion on 2D collagen I and causes cell scattering in 3D collagen I via an increase in MT1-MMP expression [37], although we found in the current study that breast cancer cells in 3D collagen I adopted Smad2 for Snail1 induction, eventually leading to cortactin suppression and aberrant localization of MT1-MMP for a less efficient metastatic potential. This study reveals that MDA-MB-231 cells embedded in 3D collagen gels and exposed to various microenvironmental parameters inactivate the JNK/c-Jun signaling pathway, which was in turn coordinated with the TGFβ1/Smad2/4 activation to promote *Snail1* transcription. This effect was observed only in cells embedded in 3D collagen gels, but not in cells

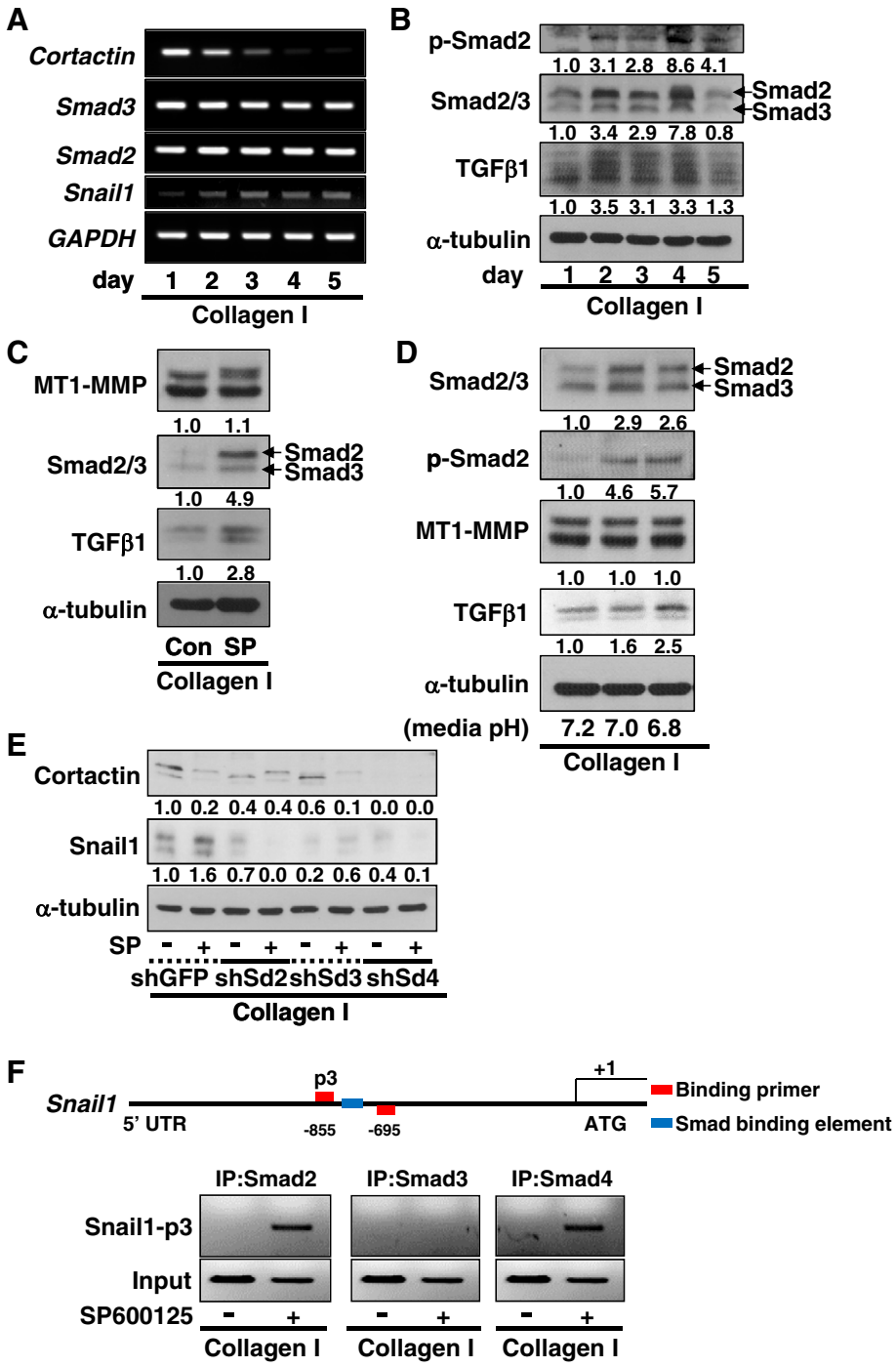

Fig. 6. Enhanced TGFβ1/Smad signaling in 3D collagen gel was responsible for increased *Snail1* transcription upon JNK signaling inhibition. (A–D) RT-PCR (A) or immunoblotting analysis (B–D) for the indicated molecules in MDA-MB-231 cells cultured in 3D collagen up to 5 days (A and B) or for 24 h (C and D), treated with vehicle (DMSO, Con) or SP600125 (SP) (C), or with culture media replenished everyday at different pH (D). (E) Immunoblots using lysates from the cells treated with DMSO (−) or SP600125 (+) after transient transfection of shGFP or shRNA against each Smad protein (shSd). (F) Schematic presentations of the Smad-binding element in the promoter regions of the *Snail1* gene (top) and ChIP assay using chromatin immunoprecipitates using anti-Smad antibodies (bottom) prepared from whole lysates of cells treated with vehicle (−) or SP600125 (+) in 3D collagen gels. The relative ratio values of band intensities were presented after normalizations to total protein (in case of phospho-protein) or α-tubulin. The data represent three independent experiments.

cultured in 2D environments, 3D Matrigel, or 3D mixture of collagen I and Matrigel, indicating a specific communication existing between the 3D microenvironment and the cells. The reduced invasiveness following cortactin suppression by Snail1 enhanced in 3D cultures surrounded with collagen I, but not with Matrigel, suggests the ECM-specific effects.

The observations in this current study may represent a unique population of breast tumor cells that shows a less effective invasion via the JNK inactivation-mediated effects, given that a small population of breast tumor cells is motile even around the margins of metastatic breast cancer models [28,29]. There are many previous reports claiming that Snail1 leads to enhanced migration and invasion [38,39]. In addition, PDGF-BB-mediated Snail1 expression in bone marrow-derived mesenchymal stem cells enhances MT1-MMP expression and invasion [40]. Breast cancer cells expressing Snail1 inoculated atop of the chorioallantoic membrane of chicks cause MT1-MMP expression and invasion [41]. Culture of fibroblasts in 3D collagen I results in a positive correlation between Snail1 and cortactin expressions for an invasive capacity

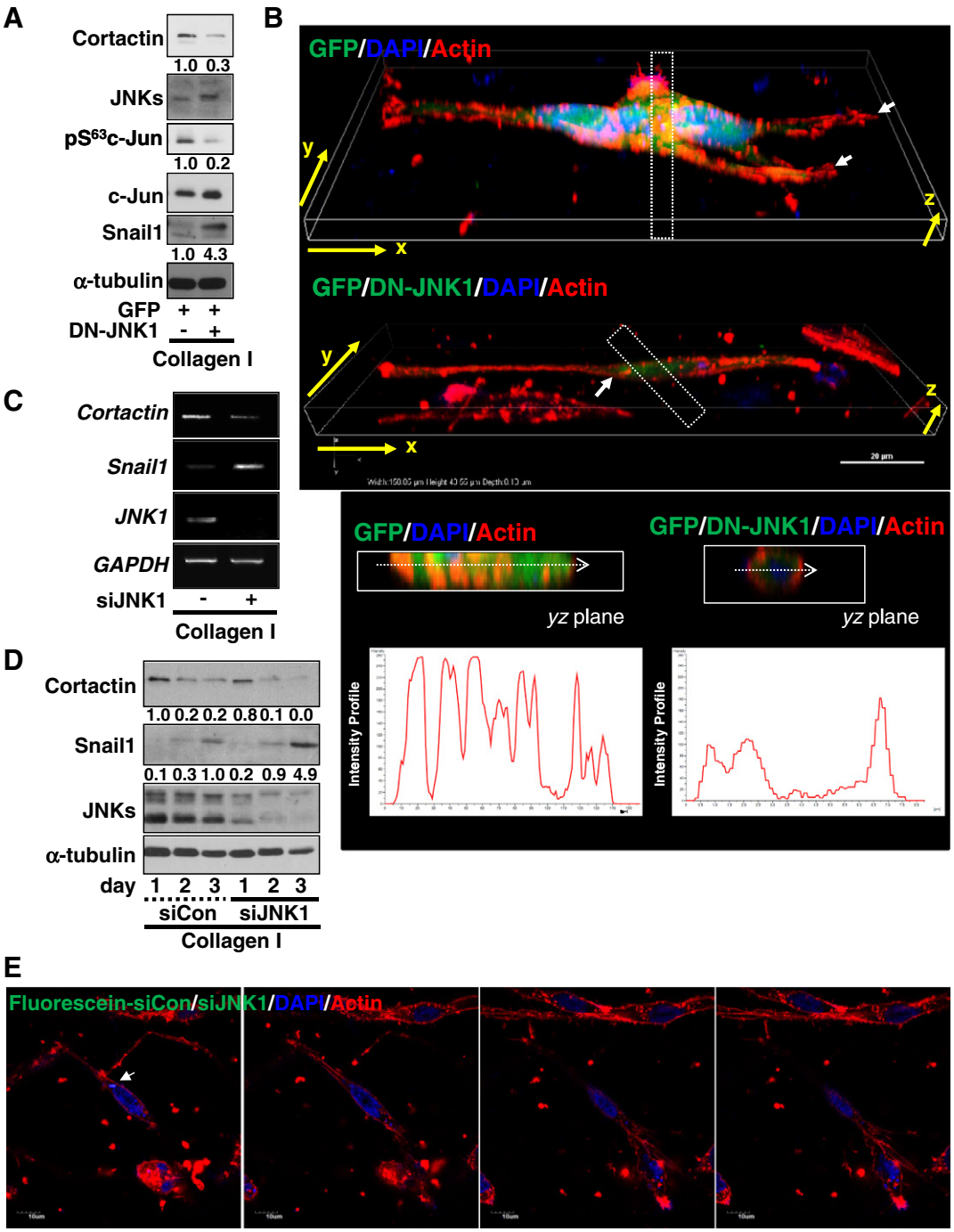

Fig. 7. JNK1 suppression caused an inverse relationship among Snail1 and cortactin expression and resulted in decreased invadopodia formation. (A and B) Immunoblots (A) or 3D-stacked images of 3D rendition (B) were processed from cells transiently transfected with empty plasmid (−) or plasmid encoding DN-JNK1 together with pEGFP (GFP) plasmid to mark the transfectants (green, B). The *yz* planes (white-dotted boxes) of confocal slices represent cut-layers for fluorescence intensity profiles, and fluorescence histograms corresponding to a section throughout the layers (white-dotted arrow) are shown to illustrate the red fluorescence peaks. (C and D) RT-PCR (C) or immunoblots (D) of cells embedded in 3D collagen gels after transient transfection with siRNAs against GFP (siGFP) or JNK1 (siJNK1). The relative ratio values of band intensities were presented after normalizations to total protein (in case of phospho-protein) or α-tubulin. (E) Cells were cotransfected with siJNK1 and fluorescein-tagged siControl for 24 h and then embedded into collagen I gels. White arrow marked siJNK1-cotransfectants with brighter blue spots by fluorescein-tagged control siRNA stains in DAPI-stained nuclei. Confocal fluorescent images of the cells were saved following DAPI and phalloidin staining for nucleus (blue) and F-actin (red), respectively. The images in serial slices were shown to compare F-actin-enriched spots between siJNK1 transfectant (arrowed) and nontransfectant (neighboring cells). The data represent three independent experiments.

[42]. The difference between these previous studies [40–42] and this current study in the effects of 3D collagen I-mediated Snail1 expression on MT1-MMP expression and invasion might be due to different cell types and/or cell culture systems.

We demonstrated here that Snail1 could suppress cortactin expression. Cortactin is an actin binding protein at actin-enriched invasive morphological features, such as invadopodia [43]. Cortactin binds to Arp2/3 actin nucleator complex during actin branching [44]. Thus, the cortactin suppression might reduce activities for actin branching processes (and thus lead to a thin cellular morphology), and presumably refractory mDia or formin-mediated fibrillar actin polymerization might lead to cellular elongations. Snail1 could bind to the *cortactin* (*CTTN*)

promoter and suppressed cortactin mRNA and protein levels only when JNK was inactivated in the cells embedded in 3D collagen gel. In addition, cortactin and MT1-MMP invadopodia markers were dynamically localized along the cellular boundaries in control cells, but enriched at perinuclear regions upon JNK inhibition or Snail1 overexpression. In this study, MT1-MMP1-enriched spots were colocalized with actin

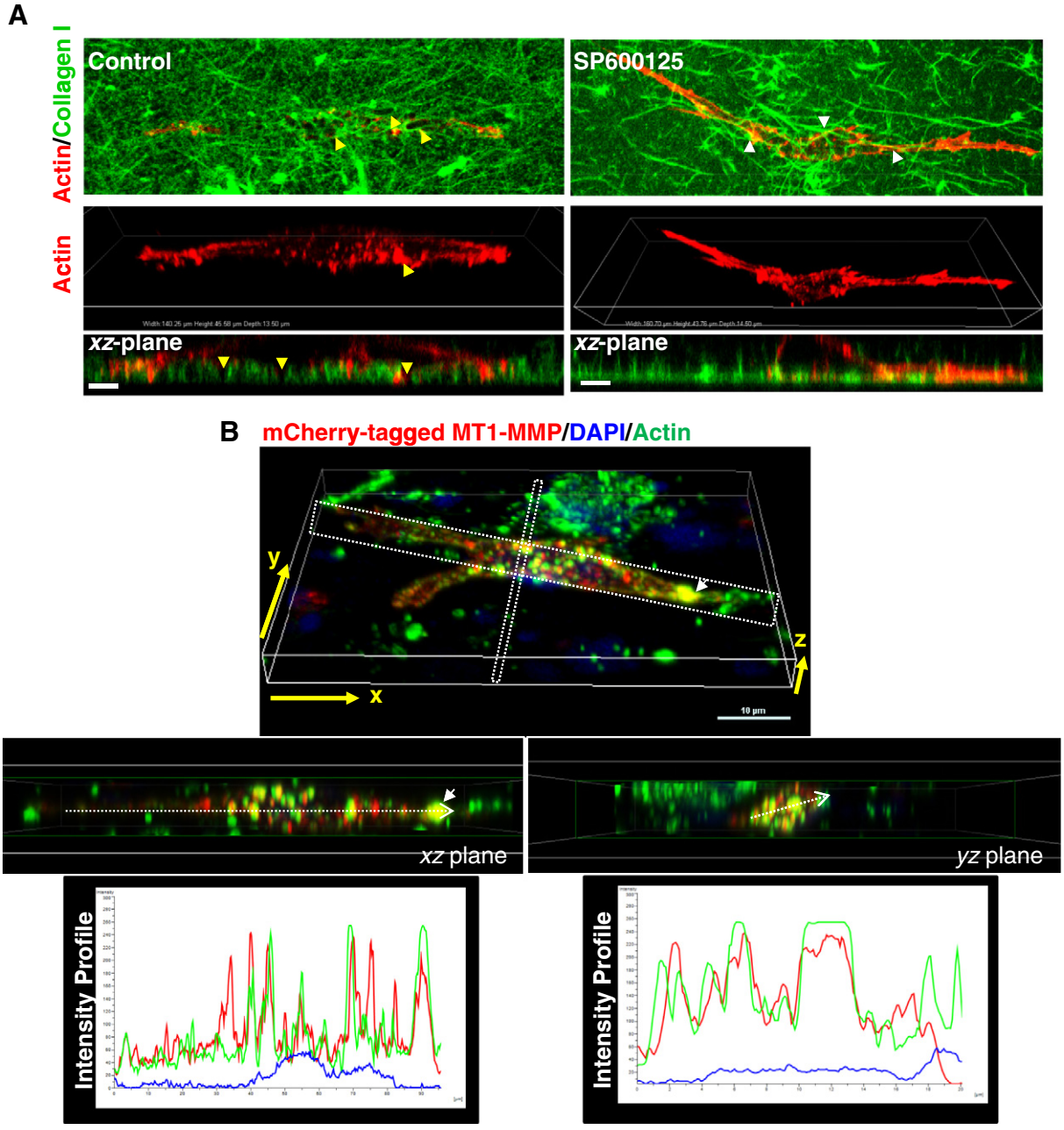

Fig. 8. Cortactin and MT1-MMP were enriched at the membrane boundaries of cells embedded in 3D collagen in a manner that was dependent on JNK signaling. (A) Cells and collagen I fibers in 3D collagen I gels were stained for actin (red) and visualized at confocal slices to see dark ECM-degraded regions (arrowheads) in the presence of DMSO (control) or SP600125 treatment. Yellow arrowheads indicated the dark area after collagen I degradation (as shown in *xz*-plane at a confocal slice), whereas white arrowheads in 600125-treated cells showed overlappings of actin and collagen I presumably without degradation of collagen I (not to be dark in *xz*-plane) during the experiment. (B–D) Cells were transiently transfected with plasmid encoding mCherry-tagged MT1-MMP for 2 days and embedded into 3D collagen I gels before staining for MT1-MMP (red) and actin (green) (B) or before live imaging for up to 4 h in the presence of DMSO (Control, C) or SP600125 (D) treatment using confocal fluorescent microscopy with a stage system kept at 37 °C and 5% CO_2. (B) The *xz* or *yz* planes (white-dotted boxes) of confocal slices represent cut-layers for fluorescence intensity profiles, and their fluorescence histograms along white-arrow sections are shown to illustrate the overlap between green fluorescence and red fluorescence, but not blue fluorescence (DAPI). (C and D) Sky-blue-dotted boxes mark the regions for the snap images and white-dotted lines indicate cellular boundaries to show alterations in cell morphology. Note that MT1-MMP positive spots in control cells show dynamic turnover along the membrane boundary (B), whereas the spots in SP600125-treated cells were stable and less frequently turnovered (C) as shown in some cases via colorful arrowheads. These snap images were from Supplementary Movies 7 (Control, C) and 8 (SP600125-treated, D). (E and F) The MDA-MB-231 cells were transfected with plasmid encoding mCherry-tagged MT1-MMP and GFP-tagged cortactin, embedded into 3D collagen gels and treated with vehicle (DMSO, Control, E) or SP600125 (F) prior to imaging for MT1-MMP (red) and cortactin (green). Arrowheads indicate regions along the membrane boundary where both cortactin and MT1-MMP localized together. Note that costained spots (yellow) are enriched in perinuclear regions of the cells treated with SP600125 (F), compared with localization on membrane boundaries in the control cells (E). These snap images were from Supplementary Movies 9 (Control, E) and 10 (SP600125-treated, F). (G—I) Cells were transiently transfected with mCherry-tagged MT1-MMP for 2 days and then embedded into 3D collagen I mixed with DQ-collagen I (at a ratio of 10:1), before live imaging using a confocal microscope at a 10 min interval. The snap images at the irregular intervals were selected from Supplementary Movies 11 (control for G) and 12 (SP600125-treated for H) to show clear differences in the green spots with ECM degradation activity (arrowheads). White dotted arrows depict directions of cell movement. mCherry-tagged MT1-MMP-transfected cells ($n = 7$ for control, $n = 6$ for SP600125-treated cells) randomly saved in multiple isolated experiments were analyzed for counting the MT1-MMP-enriched spots costained with DQ-collagen I degradation. The mean ± standard deviation values were presented as a graph (I). * depicts $p < 0.05$ for a statistical significance. The data represent three isolated experiments.

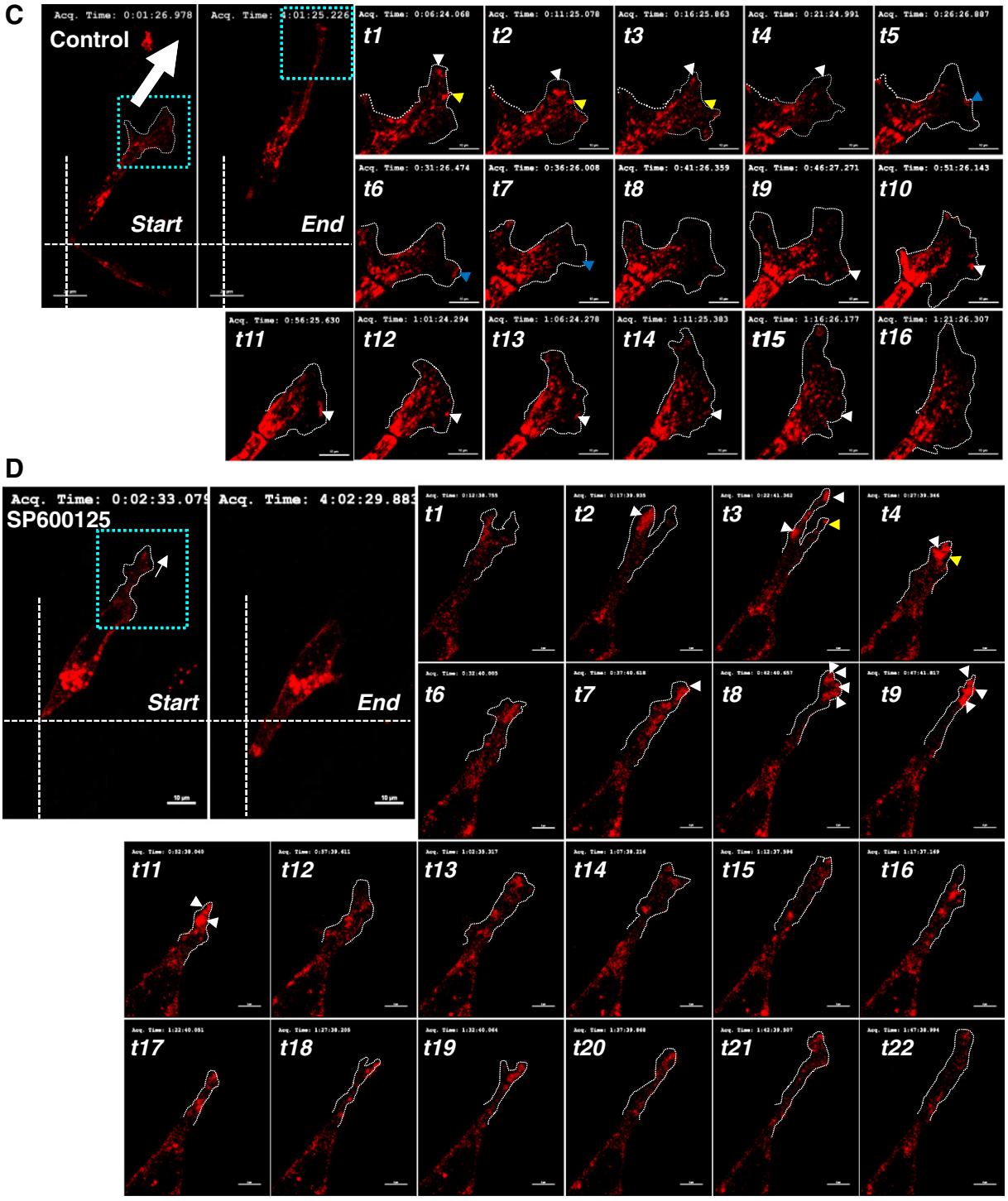

Fig. 8 (*continued*).

(Fig. 3A) and 3D ECM degradation spots along cell length or base/body (Fig. 8G), and were also costained with cortactin (Fig. 8E). Thus, the invadopodia enriched with F-actin, cortactin, and MT1-MMP to degrade surrounding collagen I were shown around flank or base/cell body area of the cells. It is also previously shown that MDA-MB-231 cells embedded in 3D environment consisting of collagen I and Matrigel for 24–36 h form invadopodia enriched with cortactin and MT1-MMP to degrade collagen along the length of and the tips of invasive protrusion [45,46]. However, it is suggested that invadopodial structures in 3D environment can be different significantly, depending on the cell types and the matrix model used [45]. The difference in the invadopodia position between the previous studies [45,46] and this current study may thus be due to differences in matrix type used and in the imaging time after the embedding (e.g., during invadopodia formation or maturation), since our MDA-MB-231 cells were embedded into collagen I gels only and imaged at 3–7 h after the embedding. Meanwhile, unlike on-top 3D systems where cells were sandwiched between two ECM layers, 3D ECM-surrounded condition in this study might have cellular morphologies more dynamic in *z*-stacks, so that the confocal images might not have a clear focus on the invasive tips of cells. In addition to the

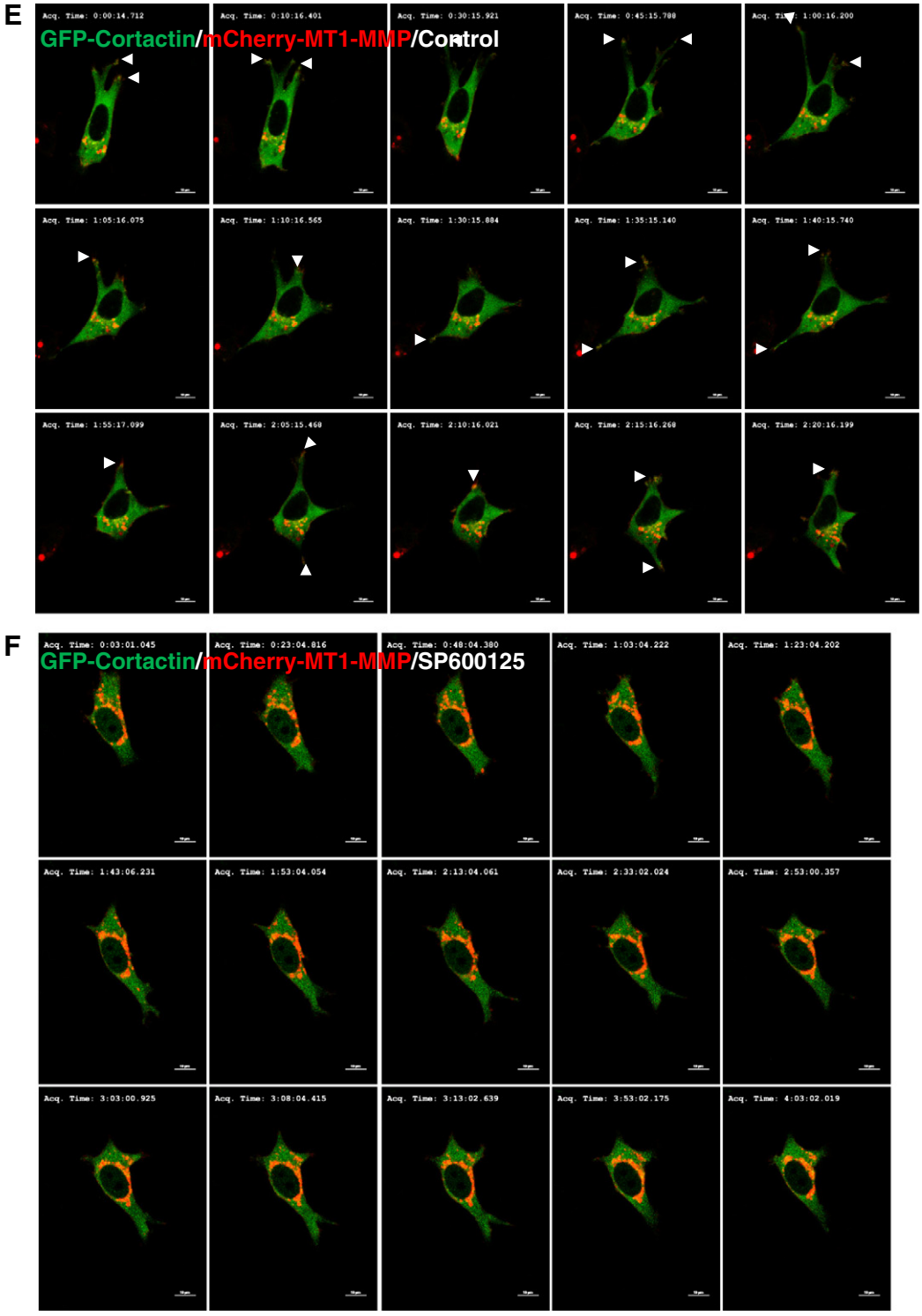

Fig. 8 (*continued*).

very tip of leading edges of migratory cells in 3D conditions, cells embedded in 3D ECM gels show invadopodia formation at the base or branching sites of protrusions during invasive path generation [47–50]. Therefore, it is suggested that the invadopodia promote ECM degradation at the very tip of and behind the leading protrusions and/or base of the cell body to generate and widen a path for invasive migration, when cells were embedded in 3D ECM conditions [51]. Thus, JNK inhibition-mediated effects (cortactin suppression and perinuclear localization of cortactin and MT1-MMP) decreased invadopodia formation and invasion in 3D collagen gels. As suggested in previous studies where Snail1 does not elicit a complete EMT [24] and that invasion is not dependent on an EMT phenotype [52], Snail1-decreased cell invasion in this study may be relevant to a specific breast cancer cell population that is maintained locally noninvasive, and whose noninvasiveness may be possible by Snail1-mediated suppression and/or abnormal localization of cortactin and/or MT1-MMP, following the JNK/c-Jun pathway inactivation via tumor cell communication with the microenvironment.

Supplementary data to this article can be found online at http://dx.doi.org/10.1016/j.bbamcr.2014.05.007.

Acknowledgements

This work was supported by the National Research Foundation of Korea (NRF) grant for the Tumor Microenvironment Global Core Research Center (GCRC) funded by the Korean government (Ministry of Science, ICT & Future Planning) (2011-0030001), for senior researchers program (Leap research, 2012-0005606/2013-035235), and for Medicinal Bioconvergence Research Center (NRF-2012M3A6A4054271) to JWL.

References

[1] P. Friedl, K. Wolf, Proteolytic interstitial cell migration: a five-step process, Cancer Metastasis Rev. 28 (2009) 129–135.
[2] S. Linder, The matrix corroded: podosomes and invadopodia in extracellular matrix degradation, Trends Cell Biol. 17 (2007) 107–117.
[3] O. Destaing, M.R. Block, E. Planus, C. Albiges-Rizo, Invadosome regulation by adhesion signaling, Curr. Opin. Cell Biol. 23 (2011) 1–10.
[4] C. Albiges-Rizo, O. Destaing, B. Fourcade, E. Planus, M.R. Block, Actin machinery and mechanosensitivity in invadopodia, podosomes and focal adhesions, J. Cell Sci. 122 (2009) 3037–3049.
[5] K.M. Yamada, E. Cukierman, Modeling tissue morphogenesis and cancer in 3D, Cell 130 (2007) 601–610.
[6] P. Friedl, E. Sahai, S. Weiss, K.M. Yamada, New dimensions in cell migration, Nat. Rev. Mol. Cell Biol. 13 (2012) 743–747.
[7] D. Hanahan, L.M. Coussens, Accessories to the crime: functions of cells recruited to the tumor microenvironment, Cancer Cell 21 (2012) 309–322.
[8] C. Box, S.J. Rogers, M. Mendiola, S.A. Eccles, Tumour-microenvironmental interactions: paths to progression and targets for treatment, Semin. Cancer Biol. 20 (2010) 128–138.
[9] M.L. Taddei, E. Giannoni, G. Comito, P. Chiarugi, Microenvironment and tumor cell plasticity: an easy way out, Cancer Lett. 341 (1) (2013) 80–96.
[10] C. Dunn, C. Wiltshire, A. MacLaren, D.A. Gillespie, Molecular mechanism and biological functions of c-Jun N-terminal kinase signalling via the c-Jun transcription factor, Cell. Signal. 14 (2002) 585–593.
[11] W. Haeusgen, T. Herdegen, V. Waetzig, The bottleneck of JNK signaling: molecular and functional characteristics of MKK4 and MKK7, Eur. J. Cell Biol. 90 (2011) 536–544.
[12] B. Derijard, M. Hibi, I.-H. Wu, T. Barrett, B. Su, T. Deng, M. Karin, R.J. Davis, JNK1: a protein kinase stimulated by UV light and Ha-Ras that binds and phosphorylates the c-JUN activation domain, Cell 76 (1994) 1025–1037.
[13] A.M. Musti, M. Treier, D. Bohmann, Reduced ubiquitin-dependent degradation of c-Jun after phosphorylation by MAP kinases, Science 275 (1997) 400–402.
[14] N.D. Ebelt, M.A. Cantrell, C.L. Van Den Berg, c-Jun N-terminal kinases mediate a wide range of targets in the metastatic cascade, Genes Cancer 4 (2013) 378–387.
[15] A. Cano, M.A. Perez-Moreno, I. Rodrigo, A. Locascio, M.J. Blanco, M.G. del Barrio, F. Portillo, M.A. Nieto, The transcription factor snail controls epithelial–mesenchymal transitions by repressing E-cadherin expression, Nat. Cell Biol. 2 (2000) 76–83.
[16] E. Batlle, E. Sancho, C. Franci, D. Dominguez, M. Monfar, J. Baulida, A. Garcia De Herreros, The transcription factor snail is a repressor of E-cadherin gene expression in epithelial tumour cells, Nat. Cell Biol. 2 (2000) 84–89.
[17] A. Villarejo, A. Cortes-Cabrera, P. Molina-Ortiz, F. Portillo, A. Cano, Differential role of Snail1 and Snail2 zinc fingers in E-cadherin repression and epithelial to mesenchymal transition, J. Biol. Chem. 289 (2014) 930–941.
[18] M.S. Lee, H.P. Kim, T.Y. Kim, J.W. Lee, Gefitinib resistance of cancer cells correlated with TM4SF5-mediated epithelial–mesenchymal transition, Biochim. Biophys. Acta 1823 (2012) 514–523.
[19] B.G. Kim, H.J. An, S. Kang, Y.P. Choi, M.Q. Gao, H. Park, N.H. Cho, Laminin-332-rich tumor microenvironment for tumor invasion in the interface zone of breast cancer, Am. J. Pathol. 178 (2011) 373–381.
[20] R.L. Klemke, Trespassing cancer cells: 'fingerprinting' invasive protrusions reveals metastatic culprits, Curr. Opin. Cell Biol. 24 (2012) 662–669.
[21] P.A. Kenny, G.Y. Lee, C.A. Myers, R.M. Neve, J.R. Semeiks, P.T. Spellman, K. Lorenz, E.H. Lee, M.H. Barcellos-Hoff, O.W. Petersen, J.W. Gray, M.J. Bissell, The morphologies of breast cancer cell lines in three-dimensional assays correlate with their profiles of gene expression, Mol. Oncol. 1 (2007) 84–96.
[22] K. Hemavathy, S.I. Ashraf, Y.T. Ip, Snail/slug family of repressors: slowly going into the fast lane of development and cancer, Gene 257 (2000) 1–12.
[23] H. Kim, M. Kang, S.A. Lee, T.K. Kwak, O. Jung, H.J. Lee, S.H. Kim, J.W. Lee, TM4SF5 accelerates G1/S phase progression via cytosolic p27(Kip1) expression and RhoA activity, Biochim. Biophys. Acta 1803 (2010) 975–982.
[24] K. Lundgren, B. Nordenskjold, G. Landberg, Hypoxia, Snail and incomplete epithelial–mesenchymal transition in breast cancer, Br. J. Cancer 101 (2009) 1769–1781.
[25] J.P. Thiery, H. Acloque, R.Y. Huang, M.A. Nieto, Epithelial–mesenchymal transitions in development and disease, Cell 139 (2009) 871–890.
[26] M.J. Blanco, G. Moreno-Bueno, D. Sarrio, A. Locascio, A. Cano, J. Palacios, M.A. Nieto, Correlation of snail expression with histological grade and lymph node status in breast carcinomas, Oncogene 21 (2002) 3241–3246.
[27] P.W. Sou, N.C. Delic, G.M. Halliday, J.G. Lyons, Snail transcription factors in keratinocytes: enough to make your skin crawl, Int. J. Biochem. Cell Biol. 42 (2010) 1940–1944.
[28] J. Condeelis, J.E. Segall, Intravital imaging of cell movement in tumours, Nat. Rev. Cancer 3 (2003) 921–930.
[29] S. Giampieri, C. Manning, S. Hooper, L. Jones, C.S. Hill, E. Sahai, Localized and reversible TGFβ signalling switches breast cancer cells from cohesive to single cell motility, Nat. Cell Biol. 11 (2009) 1287–1296.
[30] S. Wu, K. Kasisomayajula, J. Peng, E. Bancalari, Inhibition of JNK enhances TGF-β1-activated Smad2 signaling in mouse embryonic lung, Pediatr. Res. 65 (2009) 381–386.
[31] M. Pessah, J. Marais, C. Prunier, N. Ferrand, F. Lallemand, A. Mauviel, A. Atfi, c-Jun associates with the oncoprotein Ski and suppresses Smad2 transcriptional activity, J. Biol. Chem. 277 (2002) 29094–29100.
[32] Q. Liu, Y. Zhang, H. Mao, W. Chen, N. Luo, Q. Zhou, X. Yu, A crosstalk between the Smad and JNK signaling in the TGF-β-induced epithelial–mesenchymal transition in rat peritoneal mesothelial cells, PLoS One 7 (2012) e32009.
[33] S. Dennler, C. Prunier, N. Ferrand, J.M. Gauthier, A. Atfi, c-Jun inhibits transforming growth factor β-mediated transcription by repressing Smad3 transcriptional activity, J. Biol. Chem. 275 (2000) 28858–28865.
[34] J.J. Ventura, N.J. Kennedy, R.A. Flavell, R.J. Davis, JNK regulates autocrine expression of TGF-beta1, Mol. Cell 15 (2004) 269–278.
[35] D. Olmeda, G. Moreno-Bueno, J.M. Flores, A. Fabra, F. Portillo, A. Cano, SNAI1 is required for tumor growth and lymph node metastasis of human breast carcinoma MDA-MB-231 cells, Cancer Res. 67 (2007) 11721–11731.
[36] K. Zhang, C.A. Corsa, S.M. Ponik, J.L. Prior, D. Piwnica-Worms, K.W. Eliceiri, P.J. Keely, G.D. Longmore, The collagen receptor discoidin domain receptor 2 stabilizes SNAIL1 to facilitate breast cancer metastasis, Nat. Cell Biol. 15 (2013) 677–687.
[37] M.A. Shields, S. Dangi-Garimella, S.B. Krantz, D.J. Bentrem, H.G. Munshi, Pancreatic cancer cells respond to type I collagen by inducing snail expression to promote membrane type 1 matrix metalloproteinase-dependent collagen invasion, J. Biol. Chem. 286 (2011) 10495–10504.
[38] A. Garcia de Herreros, J. Baulida, Cooperation, amplification, and feed-back in epithelial–mesenchymal transition, Biochim. Biophys. Acta 1825 (2012) 223–228.
[39] C. Chiang, K. Ayyanathan, Snail/Gfi-1 (SNAG) family zinc finger proteins in transcription regulation, chromatin dynamics, cell signaling, development, and disease, Cytokine Growth Factor Rev. 24 (2013) 123–131.
[40] C. Lu, X. Sun, L. Sun, J. Sun, Y. Lu, X. Yu, L. Zhou, X. Gao, Snail mediates PDGF-BB-induced invasion of rat bone marrow mesenchymal stem cells in 3D collagen and chick chorioallantoic membrane, J. Cell. Physiol. 228 (2013) 1827–1833.
[41] I. Ota, X.Y. Li, Y. Hu, S.J. Weiss, Induction of a MT1-MMP and MT2-MMP-dependent basement membrane transmigration program in cancer cells by Snail1, Proc. Natl. Acad. Sci. U. S. A. 106 (2009) 20318–20323.
[42] R.G. Rowe, X.Y. Li, Y. Hu, T.L. Saunders, I. Virtanen, A. Garcia de Herreros, K.F. Becker, S. Ingvarsen, L.H. Engelholm, G.T. Bommer, E.R. Fearon, S.J. Weiss, Mesenchymal cells reactivate Snail1 expression to drive three-dimensional invasion programs, J. Cell Biol. 184 (2009) 399–408.
[43] L. Buday, J. Downward, Roles of cortactin in tumor pathogenesis, Biochim. Biophys. Acta 1775 (2007) 263–273.
[44] A.M. Weaver, J.E. Heuser, A.V. Karginov, W.L. Lee, J.T. Parsons, J.A. Cooper, Interaction of cortactin and N-WASp with Arp2/3 complex, Curr. Biol. 12 (2002) 1270–1278.
[45] M.A. Magalhaes, D.R. Larson, C.C. Mader, J.J. Bravo-Cordero, H. Gil-Henn, M. Oser, X. Chen, A.J. Koleske, J. Condeelis, Cortactin phosphorylation regulates cell invasion through a pH-dependent pathway, J. Cell Biol. 195 (2011) 903–920.
[46] B.T. Beaty, V.P. Sharma, J.J. Bravo-Cordero, M.A. Simpson, R.J. Eddy, A.J. Koleske, J. Condeelis, β1 integrin regulates Arg to promote invadopodial maturation and matrix degradation, Mol. Biol. Cell 24 (2013) 1661–1675 (S1661–1611).
[47] K. Wolf, Y.I. Wu, Y. Liu, J. Geiger, E. Tam, C. Overall, M.S. Stack, P. Friedl, Multi-step pericellular proteolysis controls the transition from individual to collective cancer cell invasion, Nat. Cell Biol. 9 (2007) 893–904.
[48] O. Tolde, D. Rosel, P. Vesely, P. Folk, J. Brabek, The structure of invadopodia in a complex 3D environment, Eur. J. Cell Biol. 89 (2010) 674–680.
[49] X. Yu, L.M. Machesky, Cells assemble invadopodia-like structures and invade into matrigel in a matrix metalloprotease dependent manner in the circular invasion assay, PLoS One 7 (2012) e30605.
[50] K. Vaskovicova, V. Zarsky, D. Rosel, M. Nikolic, R. Buccione, F. Cvrckova, J. Brabek, Invasive cells in animals and plants: searching for LECA machineries in later eukaryotic life, Biol. Direct 8 (2013) 8.
[51] H. Yamaguchi, Pathological roles of invadopodia in cancer invasion and metastasis, Eur. J. Cell Biol. 91 (2012) 902–907.
[52] A. Kovacs, J. Dhillon, R.A. Walker, Expression of P-cadherin, but not E-cadherin or N-cadherin, relates to pathological and functional differentiation of breast carcinomas, Mol. Pathol. 56 (2003) 318–322.